NASA TECHNICAL NOTE

NASA TN D-4601

NASA TN D-4601

C. 1

TRANSIENT THERMODYNAMIC ANALYSIS OF A FUEL-CELL SYSTEM

by William Emile Simon

Manned Spacecraft Center
Houston, Texas

NATIONAL AERONAUTICS AND SPACE ADMINISTRATION • WASHINGTON, D. C. • JUNE 1968

NASA TN D-4601

TRANSIENT THERMODYNAMIC ANALYSIS OF A FUEL-CELL SYSTEM

By William Emile Simon

Manned Spacecraft Center
Houston, Texas

NATIONAL AERONAUTICS AND SPACE ADMINISTRATION

For sale by the Clearinghouse for Federal Scientific and Technical Information
Springfield, Virginia 22151 – CFSTI price $3.00

ABSTRACT

This report presents a transient thermodynamic analysis of a fuel-cell system exclusive of cryogenic supply system and external heat dissipation system. The results of a simplified analysis and of a more general analysis are compared, and the results of the more general analysis are compared with performance test data. The analysis is oriented toward a particular application, but the methods employed are sufficiently general to allow application of these concepts to most fluid-loop systems involving heat and mass transfer.

CONTENTS

Section	Page
SUMMARY	1
INTRODUCTION	1
SYMBOLS	3
OPERATING PRINCIPLES AND CHARACTERISTICS OF THE FUEL CELL	9
DESCRIPTION OF FUEL-CELL SYSTEM SELECTED FOR ANALYSIS	17
GENERAL ANALYTICAL APPROACH	22
Type of Transient Analysis	23
Current Variations	25
Fuel-Cell Environment Temperature	25
Thermal Mass	25
Chemical Equilibrium	25
Stoichiometry	26
Perfect-Gas Law	26
Condenser-Exit-Temperature Variations	26
Pressure Conditions	26
Primary-Loop Volumetric Flow Rate And Efficiency of Water Separation	27
Performance Degradation	27
Reactant Inlet Temperature	27
Homogeneity of Hydrogen and Water-Vapor Mixture	27
DEVELOPMENT OF GOVERNING EQUATIONS	27
SIMPLIFIED TRANSIENT ANALYSIS	39

Section Page

GENERAL TRANSIENT ANALYSIS 41

Case I 49

Case II 53

Case III 57

Case IV 58

Case V 59

COMPARISON OF ANALYTICAL RESULTS 60

CONCLUDING REMARKS 63

APPENDIX A - DEVELOPMENT OF EMPIRICAL RELATION FOR FUEL-CELL POWER PLANT OUTPUT VOLTAGE AS A FUNCTION OF CURRENT, TEMPERATURE, AND ELECTROLYTE CONCENTRATION 66

APPENDIX B - THE COMPUTER PROGRAM FOR THE GENERAL ANALYSIS 71

REFERENCES 81

TABLES

Table		Page
I	CASES CONSIDERED IN THE DEVELOPMENT OF THE TRANSIENT EQUATIONS FOR DIFFERENT CURRENT AND TEMPERATURE REGIONS OF OPERATION	49

FIGURES

Figure		Page
1	Fuel-cell heat and mass balance	10
2	Energy diagram for the fuel cell	11
3	Hydrogen-oxygen fuel-cell performance based on equilibrium conditions	12
4	Fuel-cell chemical balance	14
5	Fuel-cell electrochemical flow schematic	15
6	Reaction mechanisms at hydrogen and oxygen electrodes	
	(a) Hydrogen electrode	16
	(b) Oxygen electrode	16
7	Apollo fuel-cell module	17
8	Energy conversion section	18
9	Accessory section — Bay I	18
10	Accessory section — Bay II	19
11	Accessory section — Bay III	19
12	Single-cell diagram illustrating cell construction	20
13	Schematic diagram of fuel-cell system	21
14	Control-volume approach to the analysis	23
15	Transient fuel-cell performance	24
16	Transient fuel-cell performance (step current increase)	24
17	Transient fuel-cell performance (step current decrease)	24
18	Fluid-flow diagram and heat balance for fuel-cell stack	
	(a) Flow diagram	29
	(b) Heat balance	29

Figure		Page
19	Specific heats at constant pressure for oxygen, hydrogen, and water vapor	32
20	Primary-bypass-valve characteristics	46
21	Comparison of results of the simplified analysis and the general analysis	60
22	Comparison of steady-state voltage-current characteristics	61
23	Comparison of results of general analysis with vacuum-chamber test data	
	(a) 159.9° F $\leq T_{c/e} \leq 166.3^\circ$ F	62
	(b) 157.0° F $\leq T_{c/e} \leq 167.1^\circ$ F	62
	(c) 158.0° F $\leq T_{c/e} \leq 165.5^\circ$ F	62
	(d) 159.5° F $\leq T_{c/e} \leq 164.5^\circ$ F	62
A-1	Comparison of polarization curves of analytical model with those of statistical test data	66
A-2	Variation of slope and Y-intercept of constant-temperature voltage lines with temperature	67
A-3	Variation of electrolyte concentration with temperature and partial pressure	69
A-4	Variation of Y-intercept of constant-temperature concentration lines with temperature	69

TRANSIENT THERMODYNAMIC ANALYSIS OF A FUEL-CELL SYSTEM

By William Emile Simon
Manned Spacecraft Center

SUMMARY

This report is concerned with the development of an analytical model capable of accurately predicting the transient-temperature and voltage-response characteristics of a fuel-cell system. The Apollo fuel-cell system was selected for analysis. For a given space mission, a complete time history of fuel-cell temperature and voltage must be obtained before launch to determine (1) whether there are sufficient reactants aboard the spacecraft available for fuel-cell consumption to complete the objectives of the mission and (2) whether fuel-cell voltage is always within the specification voltage band of 29 ± 2 volts. The amount of reactants consumed depends on the efficiency of the fuel cell, which is a function of operating temperature.

To obtain the necessary relations for the variation of fuel-cell temperature and voltage with time, a control volume was set up around the fuel-cell stack, which is the heart of the system. Heat and mass balances were performed, and appropriate boundary and initial conditions were applied. Because of the complexity of the system, it was necessary to introduce a set of simplifying assumptions to hold the number of varying parameters to a minimum. Some empirical (test) data were also needed.

After the transient equations were developed for all regions of normal operation, these relationships were used to formulate a computer program which accepts a given mission profile and calculates the temperature and voltage variations of the fuel cell with time.

From a comparison of analytical results with test data obtained on a qualified Apollo fuel-cell power plant in a thermal vacuum environment, it was concluded that the analysis presents an adequate mathematical model for predicting fuel-cell performance, subject to the limitations imposed on the study.

INTRODUCTION

Analytical techniques directed toward the prediction of system performance are important in the design of all systems. The prediction of the operating characteristics of the system is based on the physical geometries of the system components and on the

behavior of the working media. When various forms of energy are converted, nonisothermal systems may result. Thus, the performance analysis may be significantly complicated because (1) the system performance is generally temperature dependent, and (2) heat transfer mechanisms may be present. Generally, a thermal analysis extends beyond the system to include the influence of the surroundings. If the system is in thermodynamic equilibrium, it is in the steady-state condition. If any of the variables of the system are changing with time, the system is in the transient state.

Accurate analysis of system performance is particularly critical for design considerations for systems such as those involved in space vehicles. This report is concerned with the development of an analysis to describe the performance of a fuel-cell system such as the one used in the Apollo spacecraft. The fuel-cell system aboard the Apollo spacecraft accepts hydrogen and oxygen from a cryogenic storage and supply system and converts these reactants electrochemically into waste heat, water, and electrical energy. A thermal-control system removes the waste heat for dissipation into space by spacecraft radiators.

The variables which govern the performance of a multicomponent fuel-cell system are numerous. Analytical treatments rely to a certain extent on empirical (test) data and are limited by necessary simplifying assumptions. The most important parameter governing the performance and life capability of this type of fuel cell is temperature. Although performance increases with increasing temperature, fuel-cell life is inversely proportional to temperature. The voltage output of the system is highly dependent on fuel-cell temperature at any given load. Since the allowable range of voltage variation is very sensitive (only ± 2 volts about a nominal 29 volts), an accurate thermal analysis is necessary to be able to predict the performance of a fuel-cell system for a given space mission.

Thermodynamic analyses of fuel-cell systems are largely limited to steady-state treatments and can generally be classified as in-house reports. A transient analysis must determine the proper relationships for the variation of fuel-cell temperature and voltage with time after a given step load change for all regions of operation. Inputs to an analysis of this type must include (1) load profiles (current as a function of time), (2) fuel-cell coolant inlet-temperature profiles, (3) reactant inlet-temperature profiles, and (4) variations in the environment temperature of the fuel-cell system. The desired outputs of the analysis are the transient temperature and the voltage response of the fuel cell in terms of such variables as electrolyte concentration.

This report presents a transient thermodynamic analysis of a fuel-cell system exclusive of cryogenic supply system and external heat dissipation system. The results of a simplified analysis and of a more general analysis are compared, and the results of the more general analysis are compared with performance test data. The analysis is oriented toward a particular application, but the methods employed are sufficiently general to allow application of these concepts to most fluid-loop systems involving heat and mass transfer.

SYMBOLS

A, a, B, b, C, c	collection of terms used in the analysis for simplification
BP1, BP2	curve fit constants for primary-bypass-valve characteristics
b_1	Y-intercept
C_1	constant used in equations (135), (137), and (138)
CAHI, CBHI, CDHI, CEHI	curve fit constants for fuel-cell performance characteristics in the high-current region, $5 \text{ A} \leq I \leq 55 \text{ A}$
CALO, CBLO, CDLO, CELO	curve fit constants for fuel-cell performance characteristics in the low-current region, $0 \leq I \leq 5 \text{ A}$
C_p	specific heat at constant pressure, $\text{Btu/lb}_m\text{-}^\circ\text{R}$
E	electromotive force of the fuel cell or module output voltage, V
E_1	initial voltage, V
E_2	second-stage or final voltage, V
E_a	actual electromotive force, V
E_{cs}	cold-side effectiveness of primary regenerator
E_{rev}	reversible electromotive force, V
E_{ss}	steady-state module voltage, V
E_v	voltage variation with current and temperature (appendix A), V
e	base of natural logarithms
G	free energy (Gibbs function), Btu
H	heat content (enthalpy of formation), $\text{Btu}/^\circ\text{R}$

HF	heat of formation of water, Btu/lb_m-H_2
h	specific enthalpy, Btu/lb_m-°R
h_{fg}	latent heat of water condensed, Btu/lb_m-H_2O
I	module current, A
I_1	initial current, A
I_2	final current after a step load change, A
I^2R	heating load, $A^2\Omega$
I_{tot}	total current, A
K_1	electrochemical constant defined by Faraday's law, A-hr/lb_m-H_2cons
K_c	correction factor for the electrolyte constant of the fuel cell, V/Δ percent H_2O above 27 percent
M	thermal mass of the fuel-cell stack, Btu/°F
MW	molecular weight, lb_m/lb-mole
m	mass, lb_m
$\dot{m}$	mass flow rate, lb_m/hr
m_l	slope
n	motor speed, rpm
P	gross electrical power output of the fuel-cell module, W
P_{elec}	I^2R loss in motor, W
P_{fw}	combination of friction and windage losses of power, W
P_{he}	combination of hysteresis and eddy-current losses of power, W

P_L	power dissipated in motor because of losses, W
P_{shaft}	shaft output power of motor, W
P_{ss}	steady-state power level, W
p	absolute (or total) pressure, psia
p_{H_2}	partial pressure of hydrogen, psia
p_w	partial pressure of water vapor, psia
Q	heat generated because of the inefficiency of the fuel cell, adjusted for the difference in temperature between incoming reactants and outgoing products, Btu/hr
QA, QB	curve fit constants for stack heat loss
Q_A	heat produced in an actual fuel cell, Btu
Q_{gen}	product of hydrogen-consumption flow rate and lower heating value, Btu/hr at 77° F and 1 atm
Q_{htr}	in-line heater power, Btu/hr
Q_L	portion of waste heat generated in actual cell because of losses, Btu/hr
Q_{recir}	heat removed by the recirculating stream through the stack, Btu/hr
Q_s	heat stored in stack, Btu/hr
Q_{stack}	stack heat loss, Btu/hr
q	heat quantity (also, in some parts of the analysis, a collection of terms used to form a discriminant), Btu
R	gas constant, ft-lb_f/lb_m-°R
$\overline{R}$	universal gas constant, ft-lb_f/lb_m-mole-°R
S	entropy, Btu/°R

s	specific entropy, $Btu/lb_m\text{-}^\circ R$
T	fuel-cell operating temperature, $^\circ F$ or $^\circ R$
T_0	reference temperature, $^\circ F$ or $^\circ R$
T_1	initial fuel-cell temperature, $^\circ F$ or $^\circ R$
T_{BPHI}	bypass temperature, high
T_{BPLO}	bypass temperature, low
$T_{c/e}$	condenser exit temperature, $^\circ F$
T_{high}	upper limit of in-line (low-power) heater temperature dead band, $^\circ F$
T_{low}	lower limit of in-line (low-power) heater temperature dead band, $^\circ F$
$T_{p/e}$	actual pump exit temperature, 170° F
T_R	temperature of the mixture entering the primary regenerator, if it is assumed that there is no heat loss in the line connecting the mixing tee and the regenerator, $^\circ F$
T_s	stack inlet temperature, $^\circ F$
T_{ss}	steady-state temperature, $^\circ F$ or $^\circ R$
t	time, hr
t_0	initial time, hr
V	volume, ft^3
$\dot{V}$	volumetric flow rate, ft^3/min
v	specific volume, ft^3/lb_m
W	work done by an actual cell, Btu or W-hr
X	the smaller of $\sum(\dot{m}C_p)_{cs}$ and $\sum(\dot{m}C_p)_{hs}$

$\alpha, \beta_1, \beta_2, \beta_3, \Gamma$	collection of terms used in the analysis for simplification
γ	specific humidity, $\frac{lb_m\ H_2O}{lb_m\ dry\ H_2}$
ΔHF_p	pressure correction at constant temperature for heat of formation of water, $Btu/lb_m\text{-}H_2$
ΔHF_T	temperature correction at constant pressure for heat of formation of water, $Btu/lb_m\text{-}H_2$
$\delta_1, \delta_2, \delta_3, \delta_4$	collection of terms used in the analysis for simplification
η_{actual}	efficiency of an actual fuel cell
η_{ideal}	efficiency of an ideal fuel cell
$\eta_{\Delta G}$	fuel-cell efficiency based on free energy
$\eta_{\Delta H}$	fuel-cell efficiency based on heat content
λ	time constant for fuel-cell transient response, hr
$\xi_1, \xi_2, \xi_3, \xi_4$	collection of terms used in the analysis for simplification
$\sum(\dot{m}C_p)_{cs}$	thermal capacity rate of cold-side stream, Btu/hr-°F
$\sum(\dot{m}C_p)_{hs}$	thermal capacity rate of hot-side stream, Btu/hr-°F
τ	torque, lb_f-in.
ϕ	fraction of stack exhaust flow rate which bypasses the primary regenerator

Subscripts:

avg	average
c/e	condenser exit, primary side
cons	consumption or consumed

cs	cold side
elec	I^2R loss in motor, $A^2\Omega$
env	environment (fig. 22 and figs. 23(a) to 23(d))
f	force, lb_f
final	final value
fw	friction and windage losses, W
gen	generated heat
gly	glycol (fig. 22 and figs. 23(a) to 23(d))
he	hysteresis and eddy-current losses, W
hs	hot side
htr	heater
i	products (fig. 1)
in	entering stack
initial	initial value
j	reactants (fig. 1)
k	heat transfer quantities of the control volume (fig. 1)
m	mass, lb_m
mix	mixture
p/e	pump-separator exit, primary loop
prod	produced
pump-sep in	pump-separator assembly input
r	pressure-jacket inlet (fig. 13)
recir	recirculation stream
recir in	recirculation stream entering stack
recir out	recirculation stream leaving stack

rev	reversible
rin	reactant(s) in
ss	steady state
stack	fuel-cell stack
T	fuel-cell operating temperature, °F or °R (in eqs. (30) and (31))
theor	theoretical
tot	total
w	water vapor

OPERATING PRINCIPLES AND CHARACTERISTICS OF THE FUEL CELL

The conversion of chemical energy to electrical energy within the fuel cell is governed by Faraday's law (ref. 1) which states that during electrolysis, or while a voltaic cell is discharging, the passage of 1 faraday (96 500 coulombs) through the circuit is accompanied by the oxidation of 1 gram-equivalent weight of matter at one electrode and the reduction of 1 gram-equivalent weight of matter at the other electrode. The fuel cell converts chemical energy into electrical energy without an intermediate step of conversion into heat. Thus, the irreversibilities associated with the conversion of heat into electrical energy are eliminated, and the fuel cell has a higher ideal efficiency than the Carnot efficiency of the conventional heat engine.

From the second law of thermodynamics, the maximum useful work (change in free energy) which can be obtained from a chemical reaction at constant temperature can be expressed mathematically (ref. 2) as

$$\Delta G = \Delta H - T\,\Delta S \tag{1}$$

where G is the free energy (Gibbs function), H is the heat content (enthalpy of formation), T is the absolute temperature, and S is entropy. The change in the enthalpy of formation for the chemical process can be expressed from the heat and mass balance (fig. 1) as

$$\Delta H = \sum_i m_i h_i - \sum_j m_j h_j \tag{2}$$

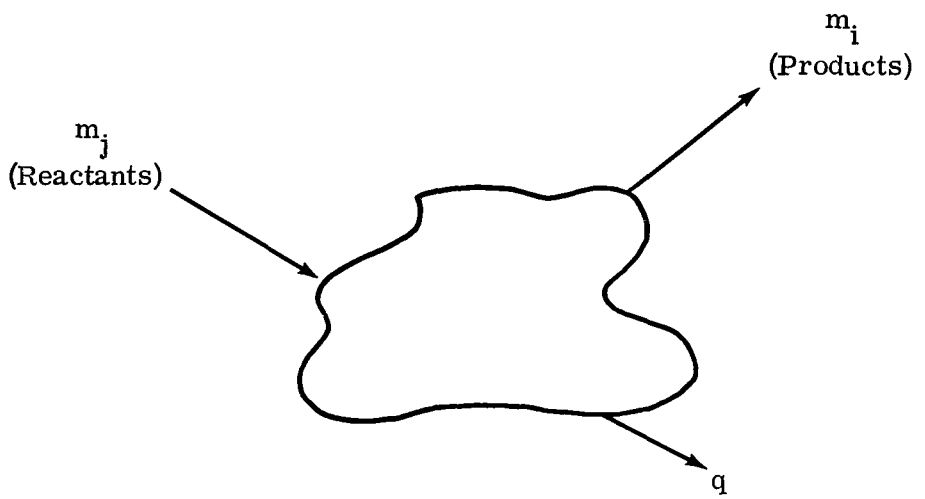

Figure 1. - Fuel-cell heat and mass balance.

If all the chemical components are at a pressure of 1 atmosphere and at a temperature of 77 ° F, then $\Delta H = q$, where q is the heat of combustion in the conventional combustion process. However, in the fuel-cell arrangement, q is converted directly into electrical energy. The change in entropy of an isothermal chemical reaction is

$$\Delta S = \sum_i m_i s_i - \sum_j m_j s_j \tag{3}$$

The efficiency of a chemical process must be evaluated differently than for the conventional heat engine. Efficiency can be defined in two ways.

$$\eta_{\Delta G} \equiv \frac{\text{actual useful work}}{\text{maximum useful work}} = \frac{\text{power} \times \text{time}}{\Delta G} \tag{4}$$

and

$$\eta_{\Delta H} \equiv \frac{\text{actual useful work}}{\text{change in heat content}} = \frac{\text{power} \times \text{time}}{\Delta H} \tag{5}$$

Since $\Delta H = \Delta G + T\,\Delta S$, $\eta_{\Delta H} < \eta_{\Delta G}$ for the same power output. This relationship is shown in figure 2.

NASA-S-67-5544

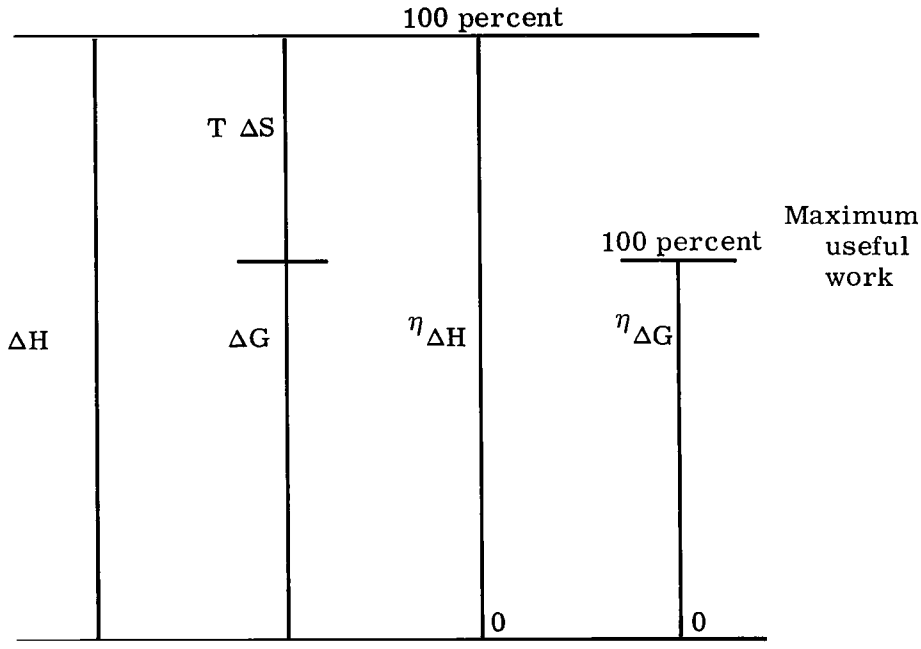

Figure 2. - Energy diagram for the fuel cell.

If the total energy based on the higher heating value (reference 14.7 psia, 77° F) could be converted into electrical energy, then a theoretical potential of 1.48 V/cell (ref. 3) could be achieved, as shown in figure 3. The theoretical potential based on the lower heating value for the same conditions is also shown for reference purposes. Because of the T ΔS limitation, the maximum theoretical potential of the cell at 14.7 psia and 77° F is 1.23 volts. This is the voltage which the cell would produce if the free energy could be converted entirely to electrical energy with no losses. The actual work in an actual fuel cell is less than the maximum useful work because of other irreversible phenomena in the physical process. Three types of irreversibilities (ref. 3) are encountered which are classified as (1) activation polarization, (2) ohmic polarization, and (3) concentration polarization. Not much is known about activation

NASA-S-67-5537

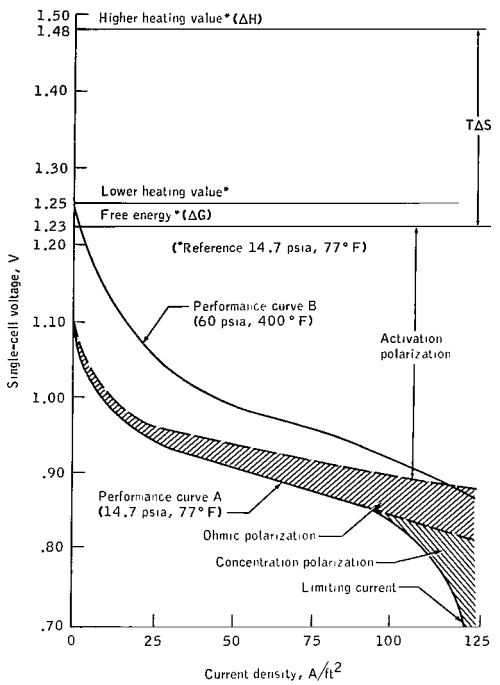

Figure 3. - Hydrogen-oxygen fuel-cell performance based on equilibrium conditions.

polarization except that it is attributed to various irreversible effects, perhaps side reactions at the fuel-cell electrodes. Ohmic polarization is caused by the electrical resistance of the electrolyte to the flow of electrons. Concentration polarization is attributed to concentration gradients within the electrolyte (caused by an increased water production rate at the electrodes) and a possible density-gradient effect within the reactant gas cavities (attributed to the presence of impurities). Because of these losses, the performance curve of an actual fuel cell would be similar to performance curve A of figure 3 for the reaction taking place at 14.7 psia and 77 ° F, with reactants and products entering and leaving under the same conditions. In figure 3, performance is expressed in terms of voltage as a function of current density, where current density is defined as the current output of the cell per unit of active cell area. The actual output power would be

$$P = EI \tag{6}$$

At higher pressures and temperatures, the maximum theoretical potential increases because of increases in free energy at higher pressure and temperature. Since the Apollo fuel cell operates at a higher temperature and pressure than the standard conditions of performance curve A, the performance of the fuel cell will be higher than indicated in performance curve A. Although it is a variable-temperature fuel cell, representative single-cell performance is given by performance curve B for 60 psia and 400° F.

The efficiency of an ideal fuel cell based on heat content ΔH (ref. 2) is

$$\eta_{ideal} = \frac{\Delta G}{\Delta H} \tag{7}$$

or, by using equation (1)

$$\eta_{ideal} = 1 - \frac{T\,\Delta S}{\Delta H} \tag{8}$$

Thus, even an ideal fuel cell operating reversibly and isothermally will have an efficiency of less than unity, and the heat quantity $T\ \Delta S$ is exchanged with the surroundings.

If all the free energy could be converted to electrical energy in the cell, then the maximum useful work would be given by

$$\Delta G = E_{rev}It \tag{9}$$

where E_{rev} is the reversible electromotive force of the cell, I is the current output, and t is the time required to consume 1 mole of fuel. Ideal efficiency then becomes

$$\eta_{ideal} = \frac{E_{rev}It}{\Delta H} \tag{10}$$

Because of the losses previously described, the waste heat produced in the actual cell Q_A is greater than the $T\ \Delta S$ heat of the ideal cell. This is expressed as

$$Q_A = T\ \Delta S + Q_L \tag{11}$$

where Q_L is that portion of the waste heat generated in the actual cell because of losses. Thus, the work done by the actual cell is

$$W = E_aIt = \Delta H - Q_A \tag{12}$$

where E_a is actual cell voltage. From equation (12), the actual cell efficiency is

$$\eta_{actual} = \frac{E_aIt}{\Delta H} = 1 - \frac{Q_A}{\Delta H} \tag{13}$$

where $Q_A > T\ \Delta S$.

The overall chemical reaction of the fuel cell is

$$2H_2 + O_2 \rightarrow 2H_2O + \text{heat} + \text{electrical energy} \tag{14}$$

Figure 4 illustrates the chemical balance within the cell which corresponds to this overall reaction. At the anode (hydrogen electrode), two hydrogen molecules are ionized to form four hydrogen ions and four electrons. The electrons travel through the external circuit and eventually reach the cathode (oxygen electrode) where they combine with one molecule of oxygen and two molecules of water (taken from the electrolyte) to form four hydroxyl ions. The four hydroxyl ions then combine with the four hydrogen ions from the anode to form four molecules of water at the hydrogen electrode. Two of the water molecules go to replenish the potassium hydroxide and water ($KOH \cdot H_2O$) electrolyte solution; the other two water molecules leave the cell as steam, having absorbed both sensible and latent heat.

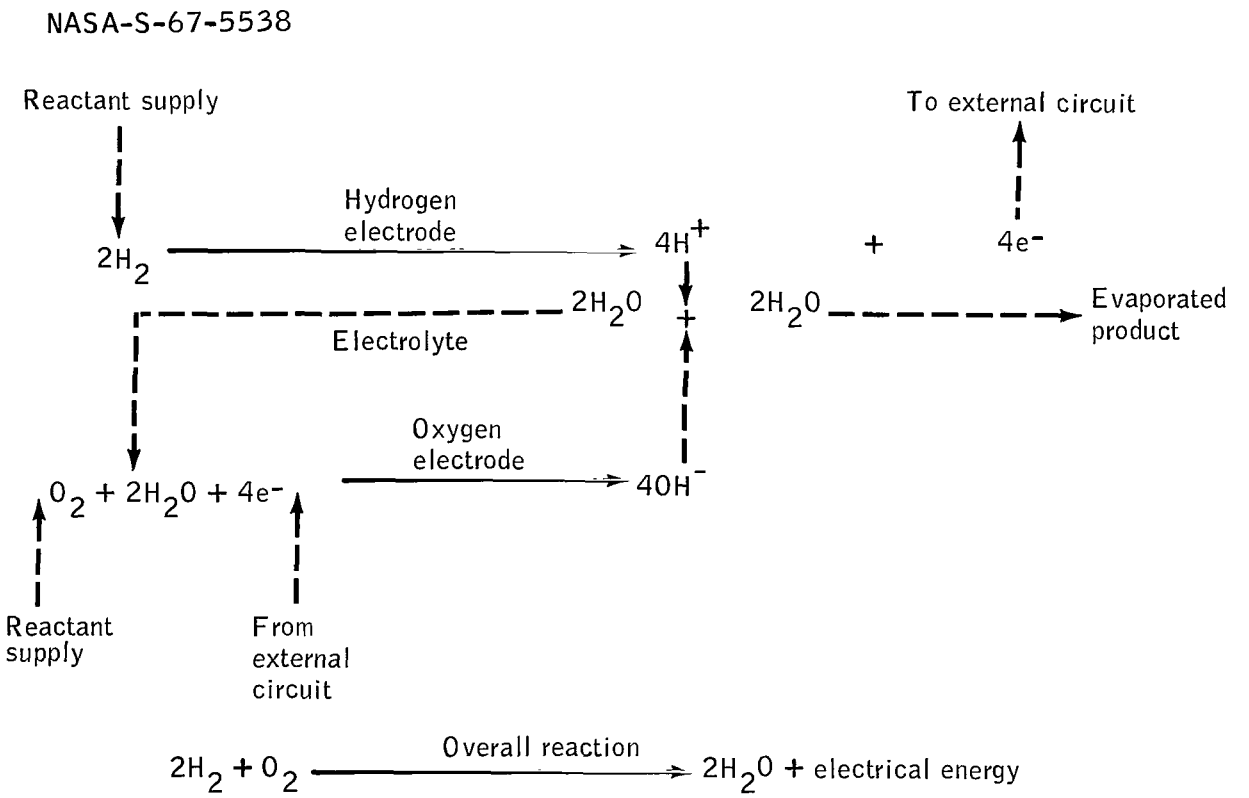

Figure 4. - Fuel-cell chemical balance.

Although the evaporated product (water) takes with it a considerable amount of heat on leaving the cell, the waste heat generated by the inefficiency of the reaction is greater than that removed by the water vapor. The excess waste heat is removed by a recirculating hydrogen stream. The recirculating hydrogen also provides a mechanism for water removal. To illustrate better the reactions and their mechanisms within the fuel cell, a cell diagram (fig. 5) is presented.

NASA-S-67-5540

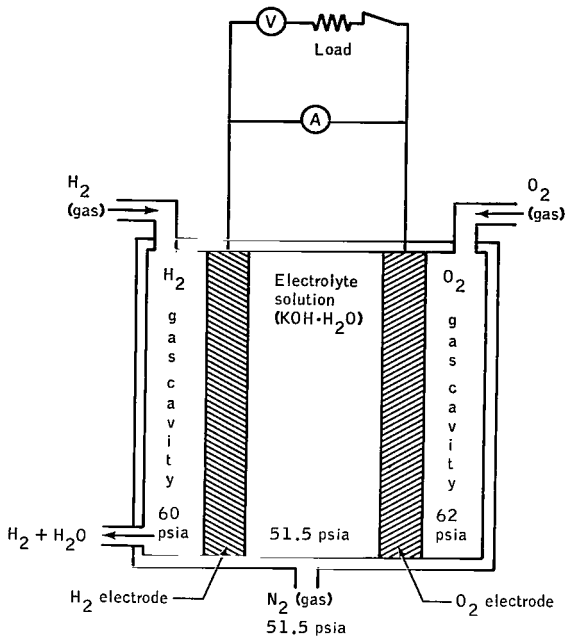

Figure 5. - Fuel-cell electrochemical flow schematic.

Hydrogen enters the hydrogen gas cavity where it reacts at the hydrogen electrode according to the equation

$$H_2 \rightleftharpoons 2H^+ + 2e^- \tag{15}$$

The hydrogen electrode potential depends on hydrogen gas pressure and hydrogen ion concentration.

The oxygen electrode reaction is

$$O_2 + 2H_2O + 4e^- \rightleftharpoons 4OH^- \tag{16}$$

The oxygen electrode potential depends on oxygen gas pressure and hydroxyl ion concentration. The total cell voltage is the difference between the hydrogen and oxygen electrode potentials.

Two reaction mechanisms exist at the hydrogen electrode. In the first mechanism, the hydrogen gas adsorbs on the dry nickel electrode surface. The adsorbed hydrogen migrates along the nickel surface until it is ionized, whereupon the hydrogen ions go into solution in the electrolyte. In the second mechanism, the hydrogen gas dissolves in the electrolyte. The dissolved hydrogen diffuses to the nickel surface, where it is ionized; the hydrogen ions then go into solution in the electrolyte. The second reaction mechanism apparently dominates.

At the oxygen electrode, the same two physical mechanisms occur as those described for the hydrogen electrode, with the second mechanism again dominating. The chemical mechanism is controversial, however, and two theories are advanced. The first (the four-electron reaction) is given by equation (16). This theory is favored for high-temperature ranges. The second theory (the Berl mechanism) holds that hydrogen peroxide ions are produced at the oxygen electrode and subsequently are decomposed at high temperatures. The chemical reactions corresponding to this theory are

$$2O_2 + 2H_2O + 4e^- \rightarrow 2OH^- + 2HO_2^- \tag{17}$$

and

$$2HO_2^- \xrightarrow[\text{high temperature}]{\text{catalyst}} 2OH^- + O_2 \tag{18}$$

or, expressed as an overall reaction

$$O_2 + 2H_2O + 4e^- \rightleftharpoons 4OH^- \tag{19}$$

The overall reaction is the same as the reaction in equation (16). The presence of hydrogen peroxide ions lowers the electrode potential, thereby contributing to cell inefficiency. However, these ions are decomposed more rapidly at higher temperatures.

Figure 6 shows schematically the reaction mechanisms occurring at the hydrogen and oxygen electrodes. The location at which the electrode, the electrolyte, and the reactant gas are all in contact is called the triple interface point.

NASA-S-67-5541

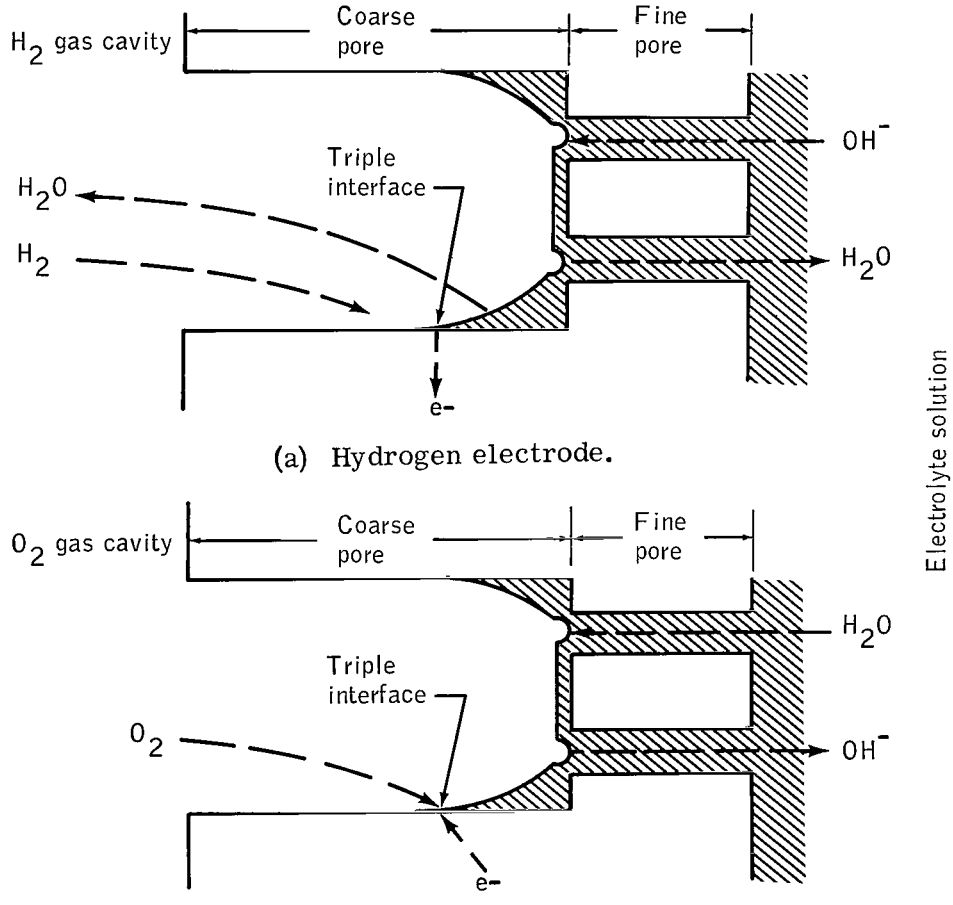

(a) Hydrogen electrode.

(b) Oxygen electrode.

Figure 6. - Reaction mechanisms at hydrogen and oxygen electrodes.

As shown in figure 6(a), the hydrogen gas flows down the coarse pore where (by one or both of the two mechanisms previously discussed) it is ionized at the triple interface. The hydrogen ions then go into solution in the electrolyte where they react with the hydroxyl ions coming from the oxygen electrode to form water. One-half of the water evaporates into the hydrogen gas. The hydrogen and water-vapor mixture then diffuses out of the coarse pore and is carried away by the hydrogen recirculation stream. The remaining water diffuses through the fine pore and into the electrolyte. Hydroxyl ions diffuse from the electrolyte, through the fine pore, to the reaction zone to replace those used up in the reaction.

As shown in figure 6(b), oxygen flows through the coarse pore to the triple interface where it reacts with water from the electrolyte and removes electrons from the nickel to become hydroxyl ions. These hydroxyl ions diffuse through the fine pore into the electrolyte to replace those used at the hydrogen electrode. Water from the electrolyte diffuses through the fine pore to the reaction site.

DESCRIPTION OF FUEL-CELL SYSTEM SELECTED FOR ANALYSIS

The Apollo fuel cell produces direct-current electrical power over a normal range of 563 to 1420 watts at a normal voltage range of 27 to 31 volts. The module (fig. 7) is 44 inches high by 22.5 inches in diameter and weighs approximately 245 pounds. Three of these modules, or power plants, connected electrically in parallel will be used in the Apollo spacecraft to provide electrical power and potable water. The module is composed of four distinct sections or systems, (1) an energy conversion section, (2) a reactant-control system, (3) a thermal-control and water-removal system, and (4) the necessary instrumentation. The last three systems are included in the accessory section.

NASA-S-67-5341

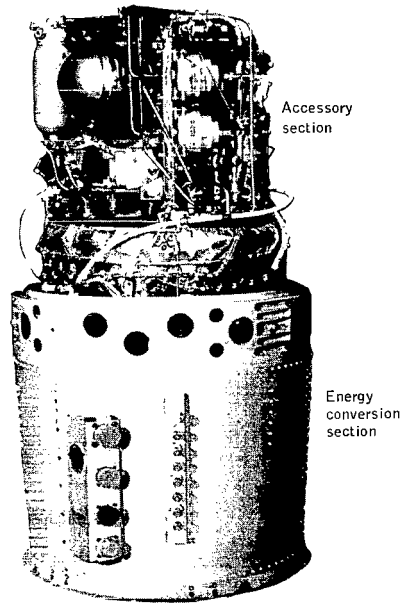

Figure 7. - Apollo fuel-cell module.

The energy conversion section is shown in figure 8. It consists mainly of a stack composed of 31 Bacon-type, series-connected cells with associated gas manifolds and connecting leads. The energy conversion section is housed in a pressurized jacket which rests in an insulated support assembly. The primary bypass valve shown in the figure will be discussed in another section of this report.

The components forming the accessory section are mounted on a Y-frame as illustrated in figure 9. The three legs of the Y-frame are 120° apart. The accessory

NASA-S-67-5342

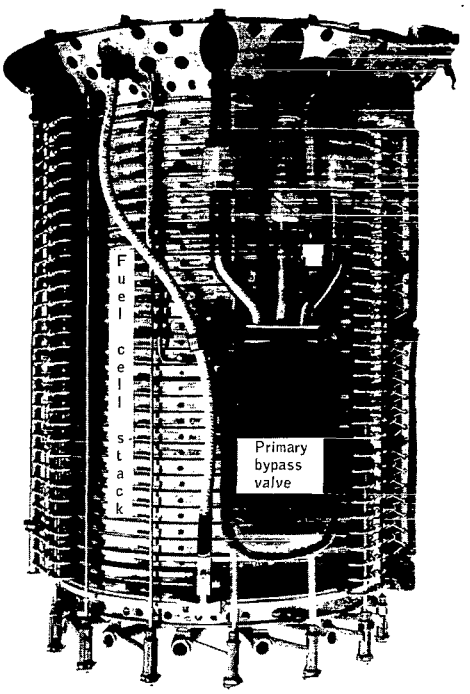

Figure 8. - Energy conversion section.

NASA-S-67-5344

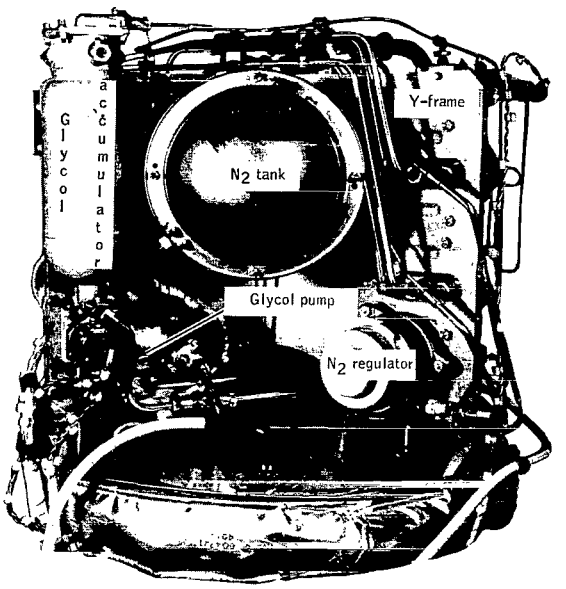

Figure 9. - Accessory section — Bay I.

section consists of a nitrogen pressurization system, three regulators, a primary loop (hydrogen and water vapor), and a secondary loop (glycol and water), as well as heat exchangers, motor-driven pumps, and plumbing. A condenser connects the two fluid loops. Figures 9, 10, and 11 show the various components of the accessory section mounted on the three legs of the Y-frame.

Before examining the system diagram, a discussion of single-cell operation would be advantageous. In figure 5, the relative pressure differentials across the electrodes are shown. The KOH · H_2O electrolyte solution is pressurized by a nitrogen blanket and regulated to 51.5 ± 0.5 psia. The reactant regulators, with the nitrogen pressure used as a reference, maintain differential pressures of 8.5 ± 0.5 psi and 10.5 ± 0.5 psi for the hydrogen and oxygen, respectively, above the nitrogen pressure. Two parameters governing the performance of the fuel-cell system are the operating pressure of the system and the relative pressure differentials across the electrodes. The pressure differential across an electrode determines the location of the triple interface previously discussed (fig. 6). By extensive testing, the combination of pressure and pressure differentials shown in figure 5 has been found to be optimum for this system from the combined standpoints of performance and operational feasibility.

NASA-S-67-5343

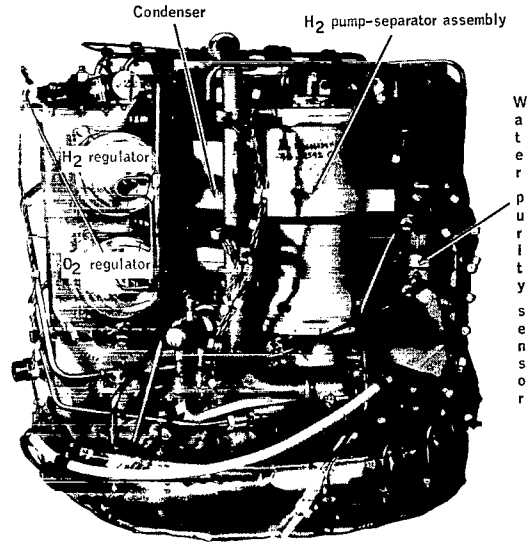

Figure 10. - Accessory section — Bay II.

NASA-S-67-5345

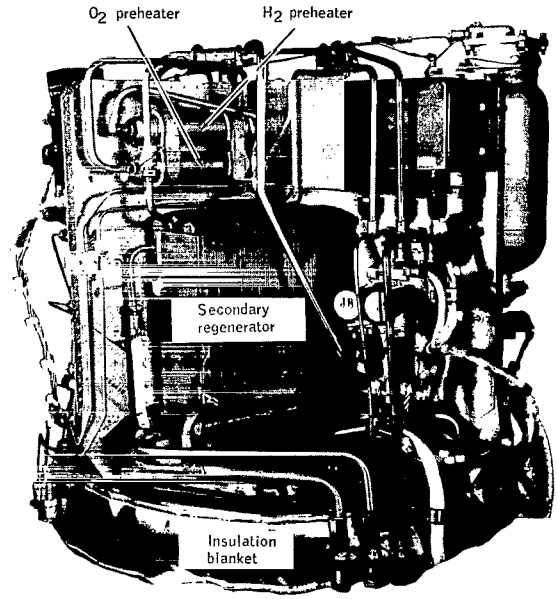

Figure 11. - Accessory section — Bay III.

Figure 12 illustrates the construction of an actual single cell. The two electrodes within each cell are composed of dual-porosity sintered nickel which is formed from nickel powder pressed into sheets. The coarse pores (approximately 40μ) are on the gas side of the electrode, and the fine pores (approximately 10μ) are on the electrolyte side. The two electrodes are similar in construction, but the oxygen electrode has a coating of black, lithium-impregnated nickel oxide on the electrolyte side to inhibit oxidation. The electrode materials serve as a catalyst in the electrochemical reaction and are resistant to corrosion by the electrolyte. A pure-nickel backup plate is used to support each electrode and also acts as a gas housing. A Teflon seal, which extends around the periphery of the cell, contains the electrolyte and acts as an electrical insulator. Although the electrodes are only about 8-1/2 inches in diameter, the entire cell is approximately 11-1/4 inches in diameter. The diaphragm section (between the electrodes and the cell spacer) accommodates changes in electrolyte concentration as the flexible backup plates expand and contract. The 31 cells are stacked in series and held together by torsion tie rods.

NASA-S-67-5542

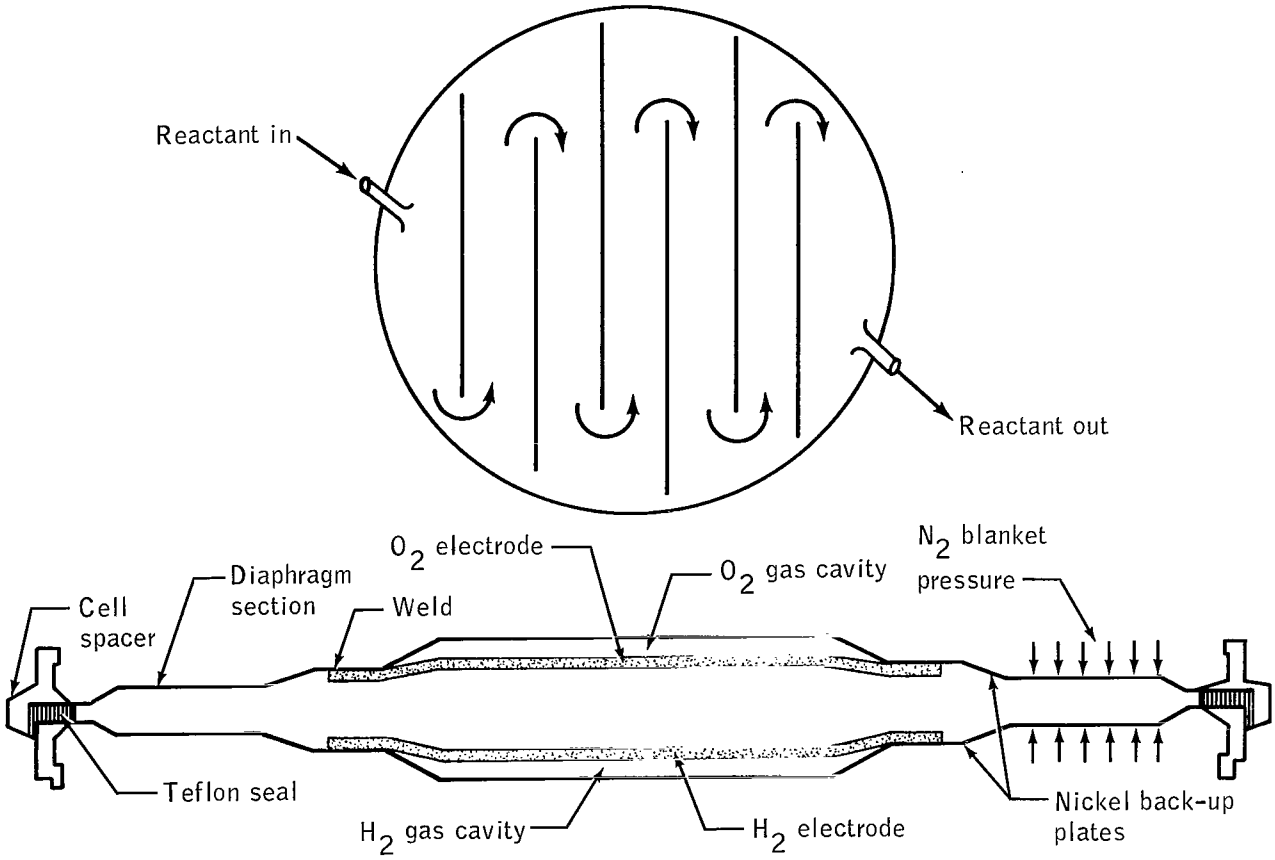

Figure 12. - Single-cell diagram illustrating cell construction.

Figure 13 is a schematic diagram of the system. Certain components not essential to the objectives of this analysis are omitted. The diagram is coded to aid in distinguishing the different fluid paths.

The nitrogen subsystem (not shown in the diagram) is composed of a small nitrogen tank (which holds approximately 0.5 lb_m of nitrogen at 1500 psia), a nitrogen regulator, and connecting lines. The regulated nitrogen pressure (51.5 ± 0.5 psia) serves a threefold purpose. It is used as a reference pressure for the hydrogen and oxygen regulators; it is used as a head pressure in the glycol accumulator; and it pressurizes the jacket around the stack, thus pressurizing the electrolyte in each of the 31 single cells.

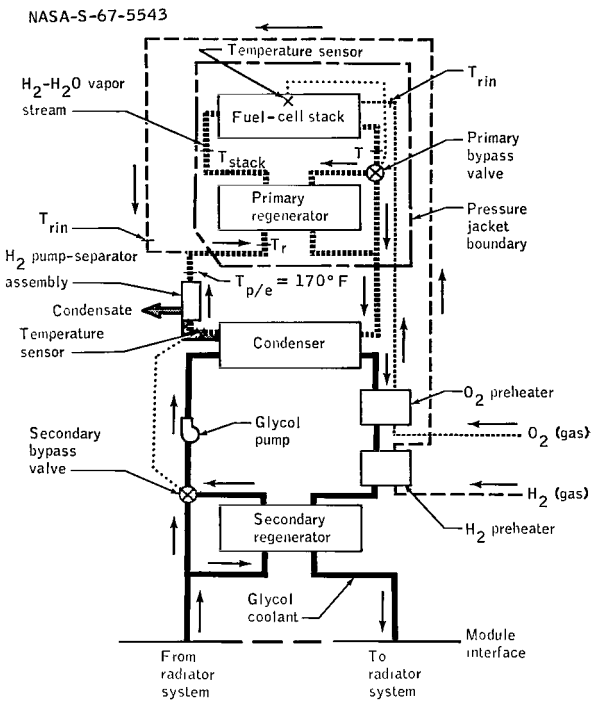

Figure 13. - Schematic diagram of fuel-cell system.

Hydrogen and oxygen are supplied to the module from a cryogenic storage system. The hydrogen is stored at a nominal 245 psia, and the oxygen is stored at a nominal 900 psia. The gases are warmed by flowing through the connecting lines between the cryogenic storage system and the fuel-cell system. Then, the gases enter the reactant preheaters before being regulated to normal operating pressures. The hydrogen and oxygen subsystems are both equipped with purge valves which, when electrically energized, permit a continuous flow of additional reactant through the cells. The surplus is dumped overboard. The purging process is performed at regular intervals to remove impurities carried into the cells by the reactants.

The makeup (or consumption) hydrogen enters the primary loop at the pump-separator exit. There it mixes with the recirculating hydrogen and water vapor and proceeds into the pressure jacket through the primary regenerator, where the mixture is heated, and from there into the stack. The primary (or hydrogen) loop consists of the primary regenerator and bypass control, the hydrogen pump-separator-motor assembly, a condenser, and an in-line heater for temperature control under low-power conditions.

The primary-bypass-valve sensor detects stack exhaust temperature, which is essentially equal to stack temperature. The sensor is a bimetallic strip that also acts as a flow diverter. Under high-power conditions when a large amount of heat must be rejected, the stack temperature is high, and the bypass valve is open (this is a proportional-control valve). Under low-power conditions when heat must be conserved, the bypass valve is closed which permits maximum regeneration.

The pump-separator is a positive-displacement (vane-type) unit. It circulates the hydrogen and water-vapor mixture through the cells to remove waste heat and product water. Liquid water from the condenser is separated from the gas stream by centrifugal action. Input power to the motor (approximately 85 watts) is supplied by three-phase, 400-cycle, 115-volt spacecraft inverters.

The condenser serves a twofold purpose. First, it maintains the primary-loop heat balance by rejecting waste heat to the glycol loop for transfer to the radiators. Second, it maintains the mass balance in the primary loop by condensing the product water vapor from the cells before this water is removed by the separator.

The secondary loop uses a coolant mixture of ethylene glycol and water. The loop consists of a glycol pump, the condenser and preheaters previously discussed, a coolant accumulator, and a secondary regenerator and bypass valve. The positive-displacement (vane-type) glycol pump circulates the coolant through the secondary-loop components and the radiator system. The desired flow characteristics are obtained by using a bypass line with an internal orifice to decrease pump flow with increasing pressure differential across the pump. Power for the pump (approximately 25 watts) is provided by the same spacecraft inverters that supply the hydrogen pump. The coolant accumulator maintains a constant pressure within the coolant system regardless of volumetric changes caused by coolant temperature variations.

The secondary regenerator controls the heat transferred from the module to the spacecraft heat-rejection system to provide the condenser with a relatively constant coolant inlet temperature. The bypass valve, which is controlled by the condenser exit temperature on the primary side, modulates the glycol flow through the cold side of the secondary regenerator. If the primary-side condenser exit temperature becomes too high, more of the glycol flow bypasses the secondary regenerator. Less of the glycol flow bypasses the secondary regenerator as the temperature goes down.

GENERAL ANALYTICAL APPROACH

The basic approach to an analysis of this type involves the formation of an analytical model for the fuel cell in a transient mode of operation, with the provision that as time t approaches infinity the model must represent the steady-state operation of the fuel-cell system. Another stipulation is that at some initial time t_0 an initial fuel-cell temperature T_1 must be known. This initial temperature is an input to the system. As indicated in figure 14, a control volume is set up around the fuel-cell stack. By analyzing the incoming and outgoing fluid streams and also the energy released within the system and transferred from it, a heat balance and a mass balance are obtained which form the basis of the analysis.

Because of the complexity of the system and the interactions of its many components, a completely theoretical approach to the transient problem would lead to a large and unwieldy set of simultaneous, higher order, nonlinear partial-differential equations. The numerical methods employed for the solution of such a set of equations would

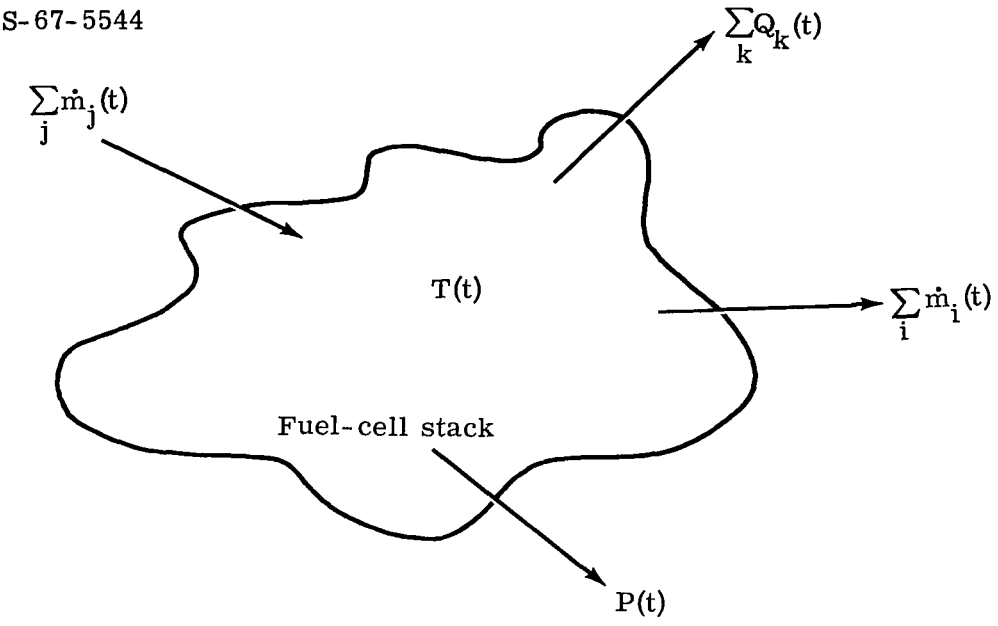

Figure 14. - Control-volume approach to the analysis.

almost certainly have stability and convergence problems which are beyond the scope of this presentation.

To circumvent these problems, an analytical approach is undertaken which uses power plant and component performance data from various tests conducted throughout the development program. This semiempirical approach, used in conjunction with a set of simplifying assumptions, aids in holding the number of varying parameters to a minimum. Thus, the governing equation for the variation of fuel-cell operating temperature with time has an exact solution. A discussion of the necessary simplifying assumptions used in the analysis follows.

Type of Transient Analysis

There are two types of transients associated with the operation of this fuel-cell system, (1) extremely short-term transients (on the order of milliseconds) and (2) long-term transients (minutes or hours). The short-term electrical transients, caused by the application of "pulse loads" or "spikes," have come and gone before the fuel-cell temperature has had time to change and, therefore, do not contribute to transient thermal effects. The long-term transients, however, are associated with a change in stack temperature and thus are the type with which this analysis will be concerned.

To illustrate the long-term thermal transient effect, consider the operating characteristics of the power plant on the polarization (voltage-current) curve in

figure 15. Suppose that the power plant is initially at a steady-state operating condition at temperature T_1, current I_1, and voltage E_1. At time t_0, a step load is applied, so that the current demand rises instantaneously from I_1 to I_2. The voltage at this instant drops from E_1 to $E_{2,\,initial}$ along the constant temperature line T_1, neglecting the short-term electrical transient. The stack is now producing a higher current. Hence, I^2R losses are greater, and the stack temperature begins to rise at a constant current I_2. If this current is maintained, temperature and voltage will approach steady-state values as t approaches infinity. As stack temperature rises, so does performance (voltage). This performance increase with time is illustrated in figure 16. Figure 17 illustrates the performance variation for a step load decrease in current.

NASA-S-67-5545

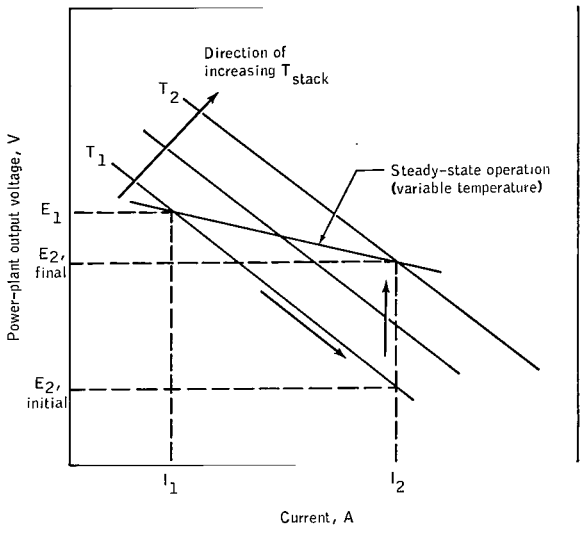

Figure 15. - Transient fuel-cell performance.

NASA-S-67-5546

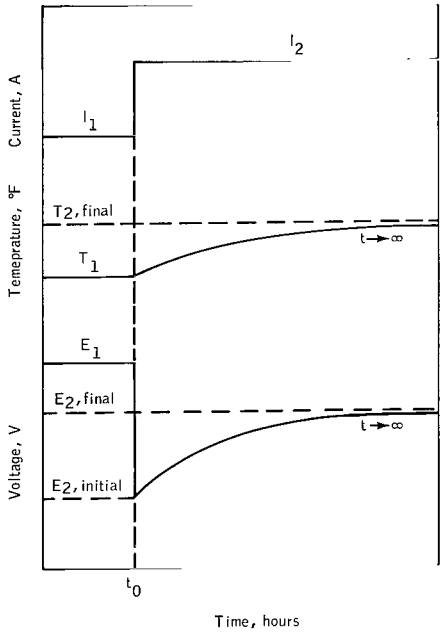

Figure 16. - Transient fuel-cell performance (step current increase).

NASA-S-67-5547

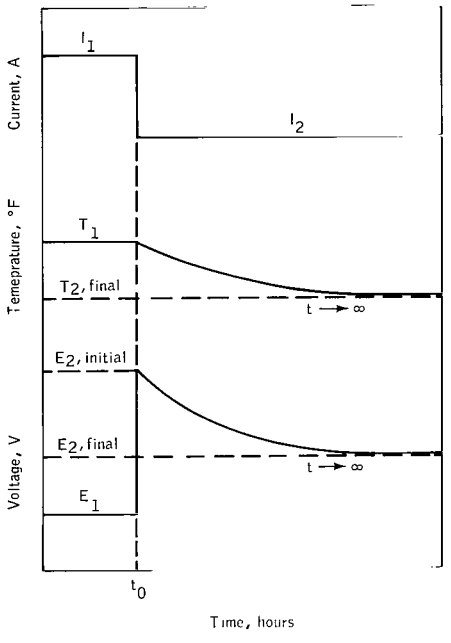

Figure 17. - Transient fuel-cell performance (step current decrease).

Current Variations

Because of the nature of most spacecraft loads, only step current variations in load are considered, with the fuel-cell output current to the spacecraft load being constant between each step load change. Actually, the current changes slightly because of fuel-cell output-voltage variations and because the voltage impressed upon a purely resistive load determines the current through it in accordance with Ohm's law.

Fuel-Cell Environment Temperature

Variations in the environment temperature of the fuel-cell module cause corresponding changes in the amount of heat lost by the module to its surroundings. These changes in heat loss affect module temperature. In this analysis, the fuel-cell environment temperature was a constant 77° F.

Thermal Mass

Since the mass of each of the primary- and secondary-loop components is almost negligible compared to the mass of the stack, it will be assumed that the thermal masses of the components and connecting lines can be neglected. This is equivalent to stating that there is no thermal time lag associated with any components other than the stack.

Chemical Equilibrium

Chemical equilibrium is defined (ref. 4) as that condition in a reversible reaction in which the speeds of the reactions in both directions are equal. The chemical equilibrium point within the cell depends on many factors, for example, the position of the triple interface at the electrodes. Three of the most important of these factors are temperature, pressure, and concentration. The analysis accounts for variations of temperature, concentration, and partial pressure of the water above the KOH in the hydrogen gas cavity. The partial pressure of the water above the electrolyte can never reach a state of equilibrium in a transient mode of operation since the concentration of the electrolyte depends on partial pressure and temperature, which are always changing. The condition of equilibrium is assumed, however, for purposes of calculating electrolyte concentration. Furthermore, since the flow rates are small and the flow paths are tortuous, it is assumed that the fluid stream leaving the stack is at the average temperature of the stack. It is also assumed that the partial pressure of the water vapor at the stack exit is equal to the average partial pressure of the water vapor in each cell. From this average stack temperature and partial pressure, an average electrolyte concentration is calculated using the previous equilibrium assumption. In other words, the concentration, temperature, and pressure gradients across the 31-cell stack are neglected.

Stoichiometry

For the chemical reaction which takes place within the cells, the condition of stoichiometry is assumed. The only two conditions which would prevent stoichiometry are (1) hydrogen diffusion through the electrolyte and (2) hydrogen or oxygen leakage from the system. Hydrogen diffusion through the electrolyte has been shown to be negligible by numerous experiments on single cells. Hydrogen leak detectors in the thermal vacuum chamber have failed to give evidence of hydrogen leakage on power plants which have been properly connected to their reactant supply systems, and oxygen containment problems are even less severe than those for hydrogen.

Perfect-Gas Law

The conditions of pressure and temperature around the primary loop are approximately 60-psia total pressure (with the partial pressure of the water vapor never exceeding 10 psia) at temperatures from 150° to 450° F. Under these conditions, the perfect-gas law (ref. 5) is satisfactory and is used throughout the analysis for the hydrogen and water-vapor mixture.

Condenser-Exit-Temperature Variations

The variation of condenser exit temperature on the primary side is always less than ±5° F from its nominal 160° F, except under adverse glycol-coolant inlet-temperature conditions. To account for these extreme variations in primary-side condenser exit temperature, a profile of module glycol inlet temperature versus time would be needed. Such a profile is not available at this time. For this reason, and because the small variations in condenser exit temperature which occur during normal operation do little to change condenser performance and cause only a very small change in the latent heat of the water condensed h_{fg}, a constant 160° F will be used for primary-side condenser exit temperature.

Pressure Conditions

Although certain very small pressure fluctuations exist from time to time in the nitrogen blanket that pressurizes the electrolyte (causing corresponding fluctuations of pressure within the hydrogen and oxygen gas cavities), a constant nitrogen pressure of 52 psia is assumed for the analysis with a constant 8.5-psid and 10.5-psid pressure differential for the hydrogen and oxygen, respectively, referenced to the nitrogen pressure as in figure 5. It is further assumed that the pressure drop in the components and connecting lines around the primary loop (a total of less than 1 psid) can be neglected. A constant total pressure of 60 psia is used for all locations in the primary loop.

Primary-Loop Volumetric Flow Rate And Efficiency of Water Separation

For primary-loop calculations, it is assumed that the volumetric flow rate of the hydrogen pump-separator assembly is constant at 3.5 ft^3/min. Although changing condensate mass flow rates at the condenser exit (caused by changing water-production rates and variations in condenser performance) cause small fluctuations in torque at the motor shaft, bench tests have shown that the pump volumetric flow rate is almost constant. These tests have also shown that the efficiency of separation of liquid water from the recirculating hydrogen and water-vapor stream is nearly 100 percent.

Performance Degradation

Because of the buildup within the cells of impurities that are carried in by the reactant gases, the power plant will experience a small degradation of voltage with time, under given conditions of current and temperature. Over the operating lifetime for which the Apollo fuel cell is qualified (400 hours), this performance degradation is statistically less than 1 percent and, therefore, will be neglected in the analysis.

Reactant Inlet Temperature

A constant reactant (hydrogen and oxygen) inlet temperature of 77° F will be used for the purposes of this analysis, since no profiles of reactant temperature versus time are as yet available. It will be evident from the analysis that unless variations in reactant inlet temperature become very extreme, performance variations are almost undetectable.

Homogeneity of Hydrogen and Water-Vapor Mixture

It will be assumed in the analysis that the recirculating hydrogen and water-vapor mixture is homogeneous throughout. Although the flow rates are fairly low, the flow regime is always turbulent because of the many bends and turns in the primary loop and because of such components as the heat exchangers, the in-line heater, and the in-line condenser-exit-temperature sensor. Therefore, a homogeneous solution is a realistic assumption. At the condenser exit, where two-phase flow exists, the gas mixture stream and the condensate stream are treated separately. In the analysis, the foregoing analytical approach is used in combination with the preceding simplifying assumptions and empirical data (where necessary).

DEVELOPMENT OF GOVERNING EQUATIONS

The analytical description of the physical behavior of fuel-cell operation is based on the proper application of the principles of conservation of mass and energy. Since the processes within the fuel cell involve chemical and phase changes and the flow of various fluids, the equations must be developed so that the number of independent variables is decreased.

For developing the reactant-consumption and water-production equations, the overall chemical reaction for the formation of water can be written as

$$H_2 + \frac{1}{2} O_2 \rightarrow H_2O \tag{20}$$

The mass balance is

$$(2.016\ lb_m)H_2 + (16\ lb_m)O_2 \rightarrow (18.016\ lb_m)H_2O \tag{21}$$

or

$$(1\ lb_m)H_2 + (7.94\ lb_m)O_2 \rightarrow (8.94\ lb_m)H_2O \tag{22}$$

With the assumption of stoichiometry, the oxygen consumption and water-production rates can be written in terms of the consumption rate of hydrogen as

$$\dot{m}_{O_2 cons} = 7.94 \dot{m}_{H_2 cons} \tag{23}$$

and

$$\dot{m}_{H_2O\ prod} = 8.94 \dot{m}_{H_2 cons} \tag{24}$$

The term reactant "consumption" is used to distinguish this quantity from total reactant usage, which is the sum of reactant consumption and purge (reactants which are vented to rid the cells of accumulated impurities).

On a time basis, Faraday's law can be used to define the electrochemical constant K_1 as

$$K_1 = \frac{96\ 500\ A}{1.008\ gm/sec\text{-}H_2 cons} = 95\ 730\ \frac{A\text{-}sec}{gm\text{-}H_2 cons} \times \frac{453.6\ gm/lb_m}{3600\ sec/hr}$$

$$= 12\ 060\ A\text{-}hr/lb_m\text{-}H_2 cons \tag{25}$$

Hence

$$\frac{1}{K_1} = 8.292 \times 10^{-5} \text{ lb}_m\text{-H}_2\text{cons/A-hr} \tag{26}$$

Therefore, by assuming stoichiometry, the hydrogen consumption rate for each of the 31 cells is

$$\dot{m}_{H_2\text{cons/cell}} = \frac{1}{K_1} I = 8.292 \times 10^{-5} I \tag{27}$$

For a 31-cell module, the consumption rate is

$$\dot{m}_{H_2\text{cons}} = 2.571 \times 10^{-3} I \tag{28}$$

Figure 18(a) is a flow diagram of the reactants, products, and recirculating stream entering and leaving the fuel-cell stack. The fluids of the recirculating stream do not enter into the chemical reaction. The consumption hydrogen enters the stack with the recirculating stream, which it joins outside the pressure jacket after passing through the hydrogen preheater. Consumption oxygen enters the stack after being conditioned in the oxygen preheater.

The stack heat loss Q_{stack}, electrical power output P, heat stored Q_s, waste heat generated Q, and the heat entering and leaving the stack by means of the recirculating stream are shown in figure 18(b). If the gases entering and leaving the stack are treated separately, the first law of thermodynamics gives

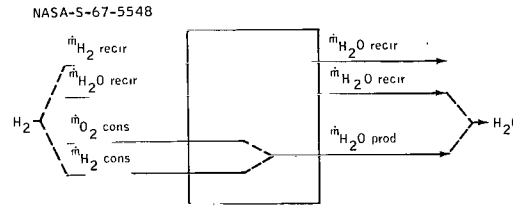

(a) Flow diagram.

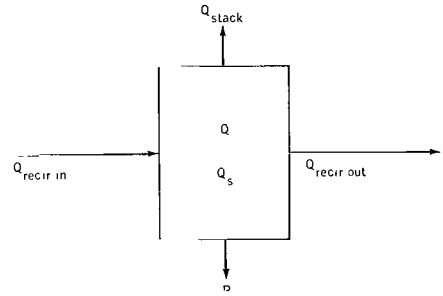

(b) Heat balance.

Figure 18. - Fluid-flow diagram and heat balance for the fuel-cell stack.

$$(\dot{m}h)_{H_2\text{cons in}} + (\dot{m}h)_{O_2\text{cons in}} + (\dot{m}h)_{H_2\text{recir in}} + (\dot{m}h)_{H_2O\text{ recir in}} + \left(\dot{m}_{H_2\text{cons}} \times HF\right)$$

$$= (\dot{m}h)_{H_2O\text{ prod out}} + (\dot{m}h)_{H_2\text{recir out}} + (\dot{m}h)_{H_2O\text{ recir out}} + 3.413P + Q_{stack} \tag{29}$$

where, for convenience, all enthalpies are referenced to 77° F. Kinetic- and potential-energy changes across the stack are negligible. The heat of formation of water HF will be taken as the lower heating value of hydrogen (since superheated steam leaves the stack) and will also be referenced to 77° F. At 1 atmosphere and 77° F (ref. 5), $HF_{77^\circ} = 51\ 571\ Btu/lb_m\text{-}H_2$.

Since the chemical reaction within the fuel cell occurs at temperatures near 400° F and at a pressure of approximately 4 atmospheres, pressure and temperature corrections should be investigated. The correction for pressure (ref. 6) is

$$\Delta HF_p = \int_{p_1}^{p_2} \left(\frac{\partial h}{\partial p}\right)_T dp \tag{30}$$

The correction for temperature (ref. 7) can be written as

$$\Delta HF_T = \int_{T_1}^{T_2} \Delta C_p \, dT \tag{31}$$

where for the reaction, $H_2(gas) + \frac{1}{2} O_2(gas) \rightarrow H_2O(gas)$

$$\Delta C_p = C_p(H_2O\ vapor) - \left[C_p(H_2\ gas) + \frac{1}{2} C_p(O_2\ gas)\right] \tag{32}$$

Since the reactants and products are treated as perfect gases, $\left(\frac{\partial h}{\partial p}\right)_T = 0$. Hence, $\Delta HF_p = 0$. The correction for temperature ΔHF_T is included in the energy balance.

The sole purpose of the recirculating stream of water vapor and hydrogen (fig. 18) is to remove heat and water. Hence, the quantity Q_{recir} is defined as the heat removed by the recirculating stream and can be written as

$$Q_{recir} = \left[(\dot{m}h)_{H_2 recir\ out} - (\dot{m}h)_{H_2 recir\ in}\right] + \left[(\dot{m}h)_{H_2O\ recir\ out} - (\dot{m}h)_{H_2O\ recir\ in}\right] \tag{33}$$

The total energy available from the heat of formation of water (before the temperature correction for HF) is

$$Q_{gen} = \dot{m}_{H_2 cons} \times HF_{77°} \tag{34}$$

By substituting equations (33) and (34) into equation (29), the energy equation becomes

$$(\dot{m}h)_{H_2 cons} + (\dot{m}h)_{O_2 cons} + Q_{gen} = (\dot{m}h)_{H_2O\ prod} + Q_{recir} + 3.413P + Q_{stack} \tag{35}$$

Introducing the net heat produced in the stack as a result of fuel-cell inefficiency Q gives

$$Q = Q_{gen} + (\dot{m}h)_{H_2 cons} + (\dot{m}h)_{O_2 cons} - (\dot{m}h)_{H_2O\ prod} - 3.413P \tag{36}$$

If equation (36) is substituted into equation (35)

$$Q = Q_{stack} + Q_{recir} \tag{37}$$

That is, the net heat generated in the stack is the sum of the stack heat loss and the heat removed by the recirculating stream. If equations (23), (24), (28), and (34) are substituted into equation (36)

$$Q = 2.57 \times 10^{-3} \frac{P}{E} \left\{ \left[\bar{C}_p(T_{in} - T_0)\right]_{H_2 cons} + 7.94 \left[\bar{C}_p(T_{in} - T_0\right]_{O_2 cons} - 8.94 \left[\bar{C}_p(T_{stack} - T_0)\right]_{H_2O\ prod} + 51\,571 \right\} - 3.413P \tag{38a}$$

where the reference temperature T_0 is 77° F. From figure 19 and reference 8, the $C_{p,avg}$ of hydrogen between 77° and 450° F is 3.44 Btu/lb_m-°R. For oxygen under these same conditions $C_{p,avg}$ = 0.221 Btu/lb_m-°R; and, similarly, for

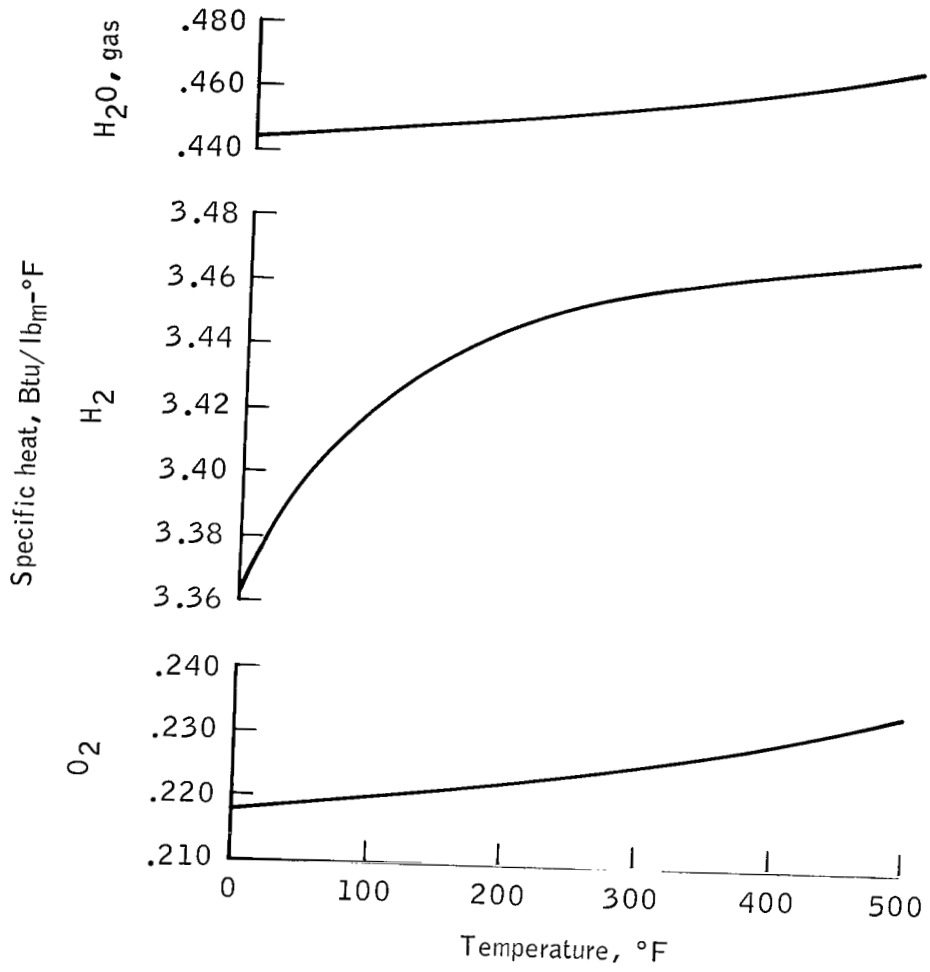

Figure 19. - Specific heats at constant pressure for oxygen, hydrogen, and water vapor.

water $C_{p,\,avg} = 0.454$ Btu/lb_m-°R. Hence, equation (38a) can be written as

$$Q = 2.57 \times 10^{-3} I \left[3.44 \left(T_{in} - 77^\circ \text{ F} \right)_{H_2 \text{cons}} + 7.94(0.221) \left(T_{in} - 77^\circ \text{ F} \right)_{O_2 \text{cons}} - 8.94(0.454) \left(T_{stack} - 77^\circ \text{ F} \right)_{H_2O \text{ prod}} + 51\,571 \right] - 3.413EI \qquad (38b)$$

By assuming $T_{H_2 in} = T_{O_2 in} = 77^\circ$ F and by denoting T_{stack} by T, equation (38b) can be reduced to

$$Q = 133.3I - 0.01043IT - 3.413EI \tag{39}$$

After a step load change (figs. 16 and 17), the fuel-cell current will be constant at I_2, and equation (39) can be rewritten as

$$Q = 133.3I_2 - 0.01043I_2T - 3.413EI_2 \tag{40}$$

To be able to solve the differential equation readily, an ordinary differential equation is desired. Therefore, the temperature and concentration gradients across the stack are neglected as a first approximation, and the only independent variable is time. Equation (40) will be used subsequently in the analysis to obtain a relationship for stack temperature as a function of time by expressing Q and E as functions of temperature and other variables.

From figure 18, for a transient thermal condition in the stack

$$Q_{recir\ in} + Q = Q_s + Q_{recir\ out} + Q_{stack} \tag{41}$$

where the fuel-cell power output P is included in the expression for Q in equation (38_a). It is assumed from calculations based on test data that the heat loss from the stack varies only linearly with temperature, that is

$$Q_{stack} = QA \cdot T + QB \tag{42}$$

where QA and QB are empirical constants. Now

$$Q_{recir\ out} - Q_{recir\ in} = \left(\dot{m}C_p\ \Delta T\right)_{H_2 recir} + \left(\dot{m}C_p\ \Delta T\right)_{H_2O\ recir} \tag{43}$$

where

$$\Delta T = T_{stack\ out} - T_{stack\ in} = T_{stack} - T_{stack\ in} = T - T_{stack\ in} \tag{44}$$

If a constant condenser exit temperature of 160° F, a constant total pressure of 60 psia, and a constant volumetric flow rate of 3.5 ft^3/min for the positive-displacement-vane pump at the condenser exit are assumed, the perfect-gas law may be applied to the fluid stream (ref. 9) as follows

$$p\dot{V} = (\dot{m}R)_{mix}T \tag{45}$$

therefore

$$(\dot{m}R)_{mix} = \frac{(60 \times 144) \times (3.5 \times 60)}{620} = 2925 \text{ Btu/hr/deg} \tag{46}$$

But

$$(\dot{m}R)_{mix} = (\dot{m}R)_{H_2} + (\dot{m}R)_{H_2O} \tag{47}$$

therefore

$$\frac{2925}{\dot{m}_{H_2 recir}} = \frac{\dot{m}_{H_2 recir} \times 767}{\dot{m}_{H_2 recir}} + \frac{\dot{m}_{H_2O\ recir} \times 85.3}{\dot{m}_{H_2 recir}} \tag{48}$$

or

$$\frac{2925}{\dot{m}_{H_2 recir}} = 767 + 85.3\gamma_{c/e} \tag{49}$$

where $\gamma_{c/e}$ = specific humidity at condenser exit $\left(lb_m\ H_2O/lb_m \text{ dry } H_2\right)$. By using the perfect-gas equation of state for each constituent of the mixture and by using Dalton's law of partial pressures

$$m_w = \frac{p_w V}{R_w T} \tag{50}$$

and

$$m_{H_2} = \frac{p_{H_2} V}{R_{H_2} T} \tag{51}$$

where the subscript w refers to water vapor and the subscript H_2 refers to dry hydrogen. Now

$$\gamma = \frac{m_w}{m_{H_2}} = \frac{p_w}{p_{H_2}} \times \frac{R_{H_2}}{R_w} = \frac{p_w}{p_{H_2}} \times \frac{\overline{R}/MW_{H_2}}{\overline{R}/MW_w} = \frac{p_w \times MW_w}{p_{H_2} \times MW_{H_2}} = \frac{p_w}{p_{H_2}} \times \frac{18.016}{2.016} = 8.94 \frac{p_w}{p_{H_2}} \tag{52}$$

But

$$p = p_{H_2} + p_w \tag{53}$$

therefore

$$p_{H_2} = p - p_w = 60 - p_w \tag{54}$$

or

$$\gamma = 8.94 \frac{p_w}{60 - p_w} \tag{55}$$

or, for later use, equation (55) can be written as

$$p_w = \frac{60}{1 + \frac{8.94}{\gamma}} \tag{56}$$

For a condenser exit temperature of 160° F, the partial pressure of the saturated water vapor is 4.741 psia, hence

$$\gamma_{c/e} = 8.94 \times \frac{4.741}{60 - 4.741} \tag{57}$$

or

$$\gamma_{c/e} = 0.767 \tag{58}$$

If equation (58) is substituted into equation (50)

$$\frac{2925}{\dot{m}_{H_2 recir}} = 767 + 85.3 \times 0.767 = 832.5 \tag{59}$$

or

$$\dot{m}_{H_2 recir} = 3.51 \text{ lb}_m/\text{hr} \tag{60}$$

therefore

$$\dot{m}_{H_2O \text{ recir}} = \gamma_{c/e} \times \dot{m}_{H_2 recir} = 0.767 \times 3.51 \tag{61}$$

or

$$\dot{m}_{H_2O \text{ recir}} = 2.70 \text{ lb}_m/\text{hr} \tag{62}$$

If equations (60) and (62) are substituted into equation (43), for the average values of specific heat stated before, and if stack inlet temperature is denoted by T_s

$$Q_{\text{recir out}} - Q_{\text{recir in}} = \left(\dot{m}C_p\,\Delta T\right)_{H_2\text{recir}} + \left(\dot{m}C_p\,\Delta T\right)_{H_2O\text{ recir}}$$

$$= (3.51)(3.44)\left(T - T_s\right) + (2.70)(0.454)\left(T - T_s\right) \qquad (63)$$

or

$$Q_{\text{recir out}} - Q_{\text{recir in}} = 13.3\left(T - T_s\right) \qquad (64)$$

The thermal mass of the stack M from test data is

$$M = 32\ \text{Btu}/^{\circ}\text{F} \qquad (65)$$

Hence, the heat quantity stored in the stack by raising the temperature of the stack from T_1 to T is

$$q_s = \int_{T_1}^{T} M\,dT = M\int_{T_1}^{T} dT = M\left(T - T_1\right) \qquad (66)$$

or

$$\frac{dq_s}{dt} = Q_s = M\frac{dT}{dt} \qquad (67)$$

Finally, if equations (42), (64), (65), and (67) are substituted into equation (41)

$$Q = 32\frac{dT}{dt} + 13.3\left(T - T_s\right) + (QA \cdot T) + QB \qquad (68)$$

or

$$Q = 32\frac{dT}{dt} + (13.3 + QA)T - 13.3T_s + QB \tag{69}$$

If equation (67) is substituted into equation (39)

$$32\frac{dT}{dt} + (13.3 + QA + 0.010431)T - 13.3T_s + (QB - 133.3I + 3.413EI) = 0 \tag{70}$$

From appendix A, if the time degradation of performance caused by the buildup of impurities is neglected, the variation of module output voltage with temperature, current, and electrolyte concentration is

$$E = (CAHI \cdot T + CBHI)I + (CDHI \cdot T + CEHI) - 0.2473(\text{percent } H_2O - 27.0) \tag{71}$$

where $360^\circ F \leq T \leq 480^\circ F$, 5 amperes $\leq I \leq$ 55 amperes, and $22 \leq$ percent $H_2O \leq 32$.

For the current region from open circuit to 5 amperes, the equation corresponding to equation (71) is

$$E = (CALO \cdot T + CBLO)I + (CDLO \cdot T + CELO) - 0.2473(\text{percent } H_2O - 27.0) \tag{72}$$

where $360^\circ F \leq T \leq 440^\circ F$, $0 \leq I \leq 5$ amperes, and $22 \leq$ percent $H_2O \leq 32$. Typical empirical values of the voltage curve fit constants are given in the following table.

High-current region	Low-current region
$CAHI = 7.96 \times 10^{-4}$ V/A-°F	$CALO = 2.775 \times 10^{-3}$ V/A-°F
CBHI = -0.481 V/A	CBLO = -1.903 V/A
CDHI = 0.026 V/°F	CDLO = 0.0157 V/°F
CEHI = 23.0 volts	CELO = 30.24 volts

Equations (70), (71), and (72) are the principal equations that describe the transient behavior of the fuel-cell system. Other expressions will be introduced, as needed, in solving these three equations for appropriate boundary and initial conditions.

SIMPLIFIED TRANSIENT ANALYSIS

A simplified transient analysis is an analysis of only the fuel-cell stack and neglects the various heat exchangers and other parts of the system. Such an analysis is developed as a first step toward mathematical formulation of the transient fuel-cell problem prior to incorporating the auxiliary components into the analysis. Although the results of the simplified analysis are not in good agreement with test data (especially at higher temperatures), they do provide satisfactory results within limits.

The energy equation for the system is equation (70). For the simplified analysis, however, the temperature T_s at which the hydrogen and water-vapor stream enters the stack (fig. 13) is assumed to be a constant 350° F; therefore, in equation (70) $\frac{dT_s}{dt} = 0$. This is equivalent to assuming the presence of a heat exchanger between the condenser exit and the stack inlet which always raises the temperature of the stream flowing through it to 350° F, regardless of other changing conditions. With this assumption, equation (70) becomes

$$32\frac{dT}{dt} + (13.3 + QA + 0.010431)T + (QB - 4655 - 133.3I + 3.413EI) = 0 \qquad (73)$$

From equation (71), if variations of electrolyte concentration with time are neglected and a constant of 27 percent water by weight is assumed for the electrolyte solution, the variation of voltage with current and temperature is

$$E = [(CAHI)T + CBHI]I + (CDHI)T + CEHI \qquad (74)$$

where 360° F $\leq$ T $\leq$ 480° F, 5 amperes $\leq$ I $\leq$ 55 amperes, and percent H_2O = 27.0. Note that the low-current region from open circuit to 5 amperes is excluded in the simplified analysis. If equation (74) is substituted into equation (73) with QA · T = 165 Btu/hr = Q_{stack} and QB = 0

$$A\frac{dT}{dt} + BT + C = 0 \qquad (75a)$$

where

$$\left.\begin{aligned} A &= 32 \\ B &= (3.413CAHI)I^2 + (3.413CDHI + 0.01043)I + 13.3 \\ C &= (3.413CBHI)I^2 + (3.413CEHI - 133.3)I - 4490 \end{aligned}\right\} \tag{75b}$$

Equation (75a) is solved by separation of variables and can be evaluated by applying the boundary condition that $T = T_1$ at $t = t_0$. The result is

$$T = -\frac{C}{B} + \left(T_1 + \frac{C}{B}\right)e^{-B/A(t - t_0)} \tag{76}$$

which is of the form

$$T = a + be^{-\lambda t} \tag{77}$$

where

$$a = -\frac{C}{B} \tag{78}$$

$$b = \left(T_1 - a\right)e^{\lambda t_0} \tag{79}$$

$$\lambda = \frac{B}{A} \tag{80}$$

The fuel-cell stack temperature T must approach its steady-state temperature T_{ss} as t becomes infinite; that is, as $t \to \infty$, $T \to T_{ss}$. When this condition is substituted into equation (78), $a = T_{ss}$. Thus, $b = \left(T_1 - T_{ss}\right)e^{\lambda t_0}$. By substituting these values of a and b into equation (77), the equation for the change in stack temperature with

time becomes

$$T = T_{ss} + \left(T_1 - T_{ss}\right)e^{\lambda t_0} \cdot e^{-\lambda t} \tag{81}$$

or

$$T = T_{ss} - \left(T_{ss} - T_1\right)e^{-\lambda\left(t-t_0\right)} \tag{82}$$

If the typical voltage curve fit constants previously stated are used, the stack temperature T_{ss} from equation (79), where $a = T_{ss}$, is given by

$$T_{ss} = \frac{1.642I^2 + 54.8I + 4490}{2.717 \times 10^{-3}I^2 + 9.91 \times 10^{-2}I + 13.3} \tag{83}$$

and the steady-state voltage is computed as

$$E_{ss} = \left(7.96 \times 10^{-4}T_{ss} - 0.481\right)I + \left(0.026T_{ss} + 23.0\right) \tag{84}$$

The steady-state power level of the fuel cell is then given by

$$P_{ss} = E_{ss} \times I \tag{85}$$

The results of this simplified analysis are compared to those of the more general transient analysis in the section on comparison of analytical results.

GENERAL TRANSIENT ANALYSIS

The analysis is extended to the general situation with the incorporation of the primary-bypass-control and primary-regenerator characteristics into the system. Although this analysis will be termed a general transient analysis, it is only general in comparison with the simplified analysis and is still subject to the simplifying assumptions in the section on general analytical approach. The incorporation of the bypass control and the primary regenerator produces a feedback effect in the temperature

region where regeneration occurs as will be shown later by comparing the results of the simplified analysis to the results of this more general analysis. This feedback effect quickens the thermal response of the system considerably in this region and narrows the operating-temperature range of the system.

In this analysis, the following assumptions previously used in the simplified analysis will be eliminated.

1. The temperature T_s at which the hydrogen and water-vapor mixture enters the stack, previously assumed to be constant, will be allowed to vary in accordance with the response of the primary bypass valve and the primary regenerator.

2. The previous assumption of constant electrolyte concentration will no longer be used. The concentration of the KOH electrolyte solution will be allowed to change according to variations in electrolyte (stack) temperature and in partial pressure of the water vapor above the KOH at the gas-electrode-electrolyte interface.

The assumption of pressure and temperature equilibrium at the gas-liquid interface will be retained for the purpose of calculating electrolyte concentration. It will further be assumed (as with stack temperature) that the partial pressure of the water vapor at the stack exit is equal to the average partial pressure of the water above the KOH within the stack.

In addition, the analysis will include the following considerations.

1. The effects of the heat input to the mixture stream at the hydrogen pump, caused by the inefficiency of the pump, are considered.

2. Thermal effects caused by the cycling of the in-line heater at low-power levels are included.

3. The low-current region (0 to 5 amperes) is included in the analysis to provide the capability of analyzing the hot-standby or no-load condition.

All previous assumptions, such as a constant condenser exit temperature of 160° F and a constant fuel-cell-system environmental temperature of 77° F, will be retained.

In the schematic diagram (fig. 13), the heat input to the system at the hydrogen pump is calculated as follows. The pump-separator motor is a three-phase, Y-connected motor that draws approximately 0.76 ampere of line current, which is equivalent to 0.76 A/phase. The spacecraft inverter supplies the motor with 115 V/phase; therefore, the motor is supplied with 87.3 V-A/phase or a total of 262 V-A for the three phases. At a nominal power factor of 0.32, the power input to the motor is approximately 84 watts.

Some of this power input is dissipated in the motor because of losses, the remainder being shaft output power. This can be expressed as

$$P_{H_2 \text{pump in}} = P_L + P_{\text{shaft}} \tag{86}$$

where P_L = power dissipated in motor because of losses, and P_{shaft} = shaft output power of motor, or P_{shaft} = shaft horsepower × 746. The power losses can be divided into three general categories, P_{fw}, P_{he}, and P_{elec}, where

$$P_L = P_{fw} + P_{he} + P_{elec} \tag{87}$$

Since the motor torque is 32.5 oz-in. at 2125 rpm

$$\text{shaft horsepower} = \frac{\tau n}{63\,060} \tag{88}$$

where τ = torque $\left(lb_f\text{-in.}\right)$, and n = motor speed (rpm), or

$$\text{shaft horsepower} = \frac{\frac{32.5}{16} \times 2125}{63\,060}$$

$$= 0.0684 \tag{89}$$

so that P_{shaft} = 51 watts. This means that P_L = 33 watts, or that the motor efficiency defined as the ratio of shaft output power to total input power is approximately 61 percent. The 51-watt equivalent of shaft horsepower operates the pump and the water separator.

The losses associated with the pump and the water separator can also be calculated. The input power to the motor can then be expressed as the sum of all these losses, plus the flow work required to pump the mixture stream around the primary loop, plus the work required to impart an amount of kinetic energy to the liquid water sufficient to remove it from the system by centrifugal force.

Regardless of the amount of the total input power converted to heat by losses, either directly or indirectly, within the pump-separator assembly, the remainder of input power will also eventually appear in the system (although not entirely in the pump-separator assembly) as heat from friction. This heat from friction, which is dissipated in other parts of the system, is only a very small part of the overall power input. It will be assumed that the total input power to the pump-separator assembly is dissipated as heat in that same assembly. Not all of this heat enters the recirculating stream, however. The fraction which is absorbed by the stream will now be calculated.

As indicated in figure 13, the temperature of the mixture stream at the pump exit is found from thermal-vacuum test data (taken from in-house performance evaluations of Apollo fuel-cell systems) to be approximately 170 ° F when the fuel-cell system is in

a nominal 77° F environment. If the small preheating effect is neglected, the reactant (makeup) hydrogen enters the primary loop at the mixing tee at a temperature of 77° F. If the specific-heat values and flow rates of the hydrogen and water vapor from the section on development of governing equations are used, the temperature to which the stream would rise if the total power input were absorbed by the stream is calculated from the following energy balance.

$$Q_{\text{pump-sep in}} = \sum(\dot{m}C_p)\left(T_{p/e} - 160^\circ\ F\right)$$

$$= \left(\dot{m}_{H_2\text{recir}} \times C_{p,\,H_2} + \dot{m}_{H_2O\ \text{recir}} \times C_{p,\,H_2O}\right)\left(T_{p/e} - 160^\circ\ F\right) \quad (90)$$

But

$$Q_{\text{pump-sep in}} = 84 \times 3.413$$

$$= 287\ \text{Btu/hr} \quad (91)$$

therefore

$$T_{p/e\ \text{theor}} = \frac{287}{(3.51 \times 3.44) + (2.70 \times 0.454)} + 160 = 181.6^\circ\ F \quad (92)$$

Since the actual temperature (from test data) to which the recirculating stream rises as it flows through the pump-separator assembly is only 170° F, the heat loss at the pump from radiation and conduction is given by

$$Q_L = \sum(\dot{m}C_p)(181.6 - 170.0) = 13.296 \times 11.6 = 154.1\ \text{Btu/hr} \quad (93)$$

Hence, the actual heat input to the recirculating stream at the pump is 132.9 Btu/hr or only about 46.3 percent of the total input power.

If the notation in figure 13 is used, the mixing equation for the hydrogen makeup tee is

$$\dot{m}_{H_2\text{cons}} \times C_{p,\,H_2} \times \left(T_{\text{rin}} - T_0\right) + \dot{m}_{H_2\text{recir}} \times C_{p,\,H_2}\left(T_{p/e} - T_0\right) + \dot{m}_{H_2O\ \text{recir}}$$

$$\times C_{p,\,H_2O}\left(T_{p/e} - T_0\right) = \dot{m}_{H_2\text{recir}} \times C_{p,\,H_2}\left(T_R - T_0\right) + \dot{m}_{H_2O\ \text{recir}}$$

$$\times C_{p,\,H_2O}\left(T_R - T_0\right) + \dot{m}_{H_2\text{cons}} \times C_{p,\,H_2}\left(T_R - T_0\right) \quad (94)$$

where T_0 is a reference temperature; T_R is the temperature of the mixture entering the primary regenerator, if it is assumed that there is no heat loss in the line connecting the mixing tee and the regenerator; and $T_{p/e}$ is the actual pump exit temperature (170° F). All terms containing the reference temperature T_0 are removed by subtraction. If equation (94) is rearranged and if the known temperatures, the flow rates, equation (28), and the specific heats are substituted into the equation, the expression for T_R is given as

$$T_R = \frac{0.681I + 2261}{8.841 \times 10^{-3} I + 13.3} \tag{95}$$

where I is fuel-cell current. It is assumed that T_R changes instantaneously with a step current change, although there is some small timelag associated with the mixing tee.

To calculate the mixture temperature at the cold-side exit of the primary regenerator T_s, the cold-side effectiveness E_{cs} of the regenerator must be considered. The effectiveness of this counter-flow heat exchanger is defined as

$$E_{cs} \equiv \frac{\sum\left(\dot{m}C_p\right)_{cs}\left(T_s - T_R\right)}{X\left(T - T_R\right)} \tag{96}$$

and

$$\sum\left(\dot{m}C_p\right)_{cs} = \left(\dot{m}C_{p,\,H_2\text{recir}}\right) + \left(\dot{m}C_{p,\,H_2\text{cons}}\right) + \left(\dot{m}C_{p,\,H_2O\text{ recir}}\right) \tag{97}$$

where $\sum\left(\dot{m}C_p\right)_{cs}$ is the thermal capacity rate of the cold-side stream, X is the smaller of $\sum\left(\dot{m}C_p\right)_{cs}$ and $\sum\left(\dot{m}C_p\right)_{hs}$, and $\sum\left(\dot{m}C_p\right)_{hs}$ is the thermal capacity rate of the hot-side stream.

To determine X, the characteristic of the primary bypass control must be introduced. Figure 20 is a plot of percent bypass versus temperature. The bypass valve is biased to stack temperature T by means of a bimetallic strip which is placed within the valve in the stack exhaust stream. Curves A and B in figure 20 illustrate the effects of hysteresis inherent in the valve. For example, if the stack temperature is at 430° F and rising, then the percent bypass follows curve A. However, if the stack temperature starts decreasing after reaching 444° F, the valve will continue to bypass 50 percent of the total flow around the regenerator until T = 441° F. At this point, the percent bypass will start to decrease along curve B.

NASA-S-67-5550

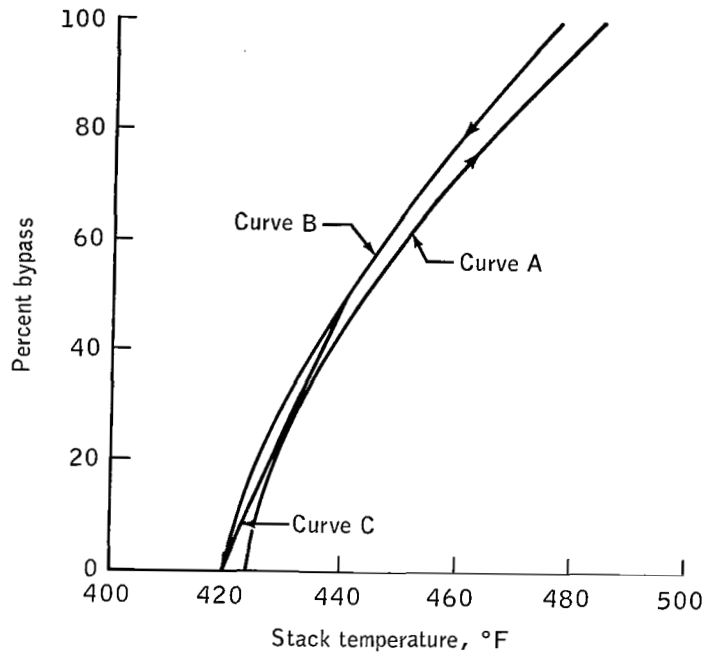

Figure 20. - Primary-bypass-valve characteristics.

Since the valve-temperature dead band caused by hysteresis is relatively small, it is neglected in this analysis. Also, since the normal operating-temperature range of the power plant is 380° to 440° F from minimum to maximum power, the linear-bypass-valve characteristic (typical) of curve C is used.

Now

$$\sum\left(\dot{m}C_p\right)_{cs} = \left(\dot{m}_{H_2}\text{recir} + \dot{m}_{H_2}\text{cons}\right) C_{p,\,H_2} + \left(\dot{m}_{H_2O}\text{ recir} \times C_{p,\,H_2O}\right)$$

$$= \left(3.51 + 2.57 \times 10^{-3}I\right) \times 3.44 + (2.70)(0.454) \tag{98}$$

or

$$\sum\left(\dot{m}C_p\right)_{cs} = 8.841 \times 10^{-3}I + 13.3 \tag{99}$$

Let the bypass fraction be denoted by ϕ; that is, ϕ = percent bypass $\times 10^{-2}$, so that

$$\sum(\dot{m}C_p)_{hs} = (1 - \phi)\left[\left(\dot{m}_{H_2}\text{recir} \times C_{p,\,H_2}\right) + \left(\dot{m}_{H_2O}\text{ recir} + \dot{m}_{H_2O}\right) \cdot C_{p,\,H_2O}\right] \tag{100}$$

where $\dot{m}_{H_2O}$ is that portion of the water produced which exits from the stack. This term can be expressed as

$$\dot{m}_{H_2O} = \dot{m}_{H_2O\text{ prod}} + \left(\frac{d\dot{m}_{H_2O}}{dt}\right) \tag{101}$$

where $\frac{d\dot{m}_{H_2O}}{dt} \leq 0$. In a steady-state condition, all the water produced leaves the stack and $\frac{d\dot{m}_{H_2O}}{dt} = 0$. Therefore, for steady-state operation

$$\dot{m}_{H_2O} = \dot{m}_{H_2O\text{ prod}} \tag{102}$$

In the transient condition, $\frac{d\dot{m}_{H_2O}}{dt} \leq 0$. But $\dot{m}_{H_2O}$ changes as electrolyte concentration (percent H_2O) changes; therefore

$$\frac{d\dot{m}_{H_2O}}{dt} = \left[\frac{d(\text{percent } H_2O)}{dt}\right]\left[\frac{d\dot{m}_{H_2O}}{d(\text{percent } H_2O)}\right] \tag{103}$$

However, since changes in electrolyte concentration are very small, this term can be neglected with only very small error; hence

$$\dot{m}_{H_2O} \approx \dot{m}_{H_2O\ prod} \tag{104}$$

The expression for the hot-side thermal capacity rate is then

$$\begin{aligned}\sum\left(\dot{m}C_p\right)_{hs} &= (1 - \phi)\left[\left(\dot{m}_{H_2 recir} \times C_{p,H_2}\right) + \left(\dot{m}_{H_2O\ recir} + \dot{m}_{H_2O\ prod}\right) \times C_{p,H_2O}\right] \\ &= (1 - \phi)\left[(3.51 \times 3.44) + \left(2.70 + 8.94 \times 2.57 \times 10^{-3}I\right)(0.454)\right] \\ &= (1 - \phi)\left(10.431 \times 10^{-3}I\right) + 13.3 \end{aligned} \tag{105}$$

or

$$\sum\left(\dot{m}C_p\right)_{hs} = (1 - \phi)\alpha \tag{106}$$

where $\alpha = \alpha(I) = 10.431 \times 10^{-3}I + 13.3$.

It is evident from the graph in figure 20 that there are two distinct stack-temperature regions to be considered; that is, the regions of variable regeneration from 360° to 420° F and from 420° to 440° F. (The upper limit used is 440° F since this temperature roughly corresponds to the temperature of the stack at its rated maximum-continuous-output power of 1420 watts.) It is also evident from appendix A that there are two current regions. Because of the various regions of current and temperature, there are five cases to be considered. These cases are listed in table I. The cut-off temperatures, 420° and 440° F, used in table I are typical; however, these values are generalized for computer programing purposes by using T_{BPLO} and T_{BPHI}, respectively.

TABLE I. - CASES CONSIDERED IN THE DEVELOPMENT OF THE TRANSIENT EQUATIONS FOR DIFFERENT CURRENT AND TEMPERATURE REGIONS OF OPERATION

Case	Current region, A		Temperature region			In-line heater	
			Regeneration				
	0 to 5	5 to 55	Full, $\phi = 0$	Partial, $\phi = 0$	Temperature range, °F	On	Off
I		X	X		$360 \leq T \leq 420$		X
II		X		X	$420 \leq T \leq 440$		X
III		X	X		$360 \leq T \leq 420$	X	
IV	X		X		$T_{high} \leq T \leq 420$		X
V	X			X	$420 \leq T \leq 440$		X

The transient equations for all cases for the variation, after a given step load change, of stack temperature with time are derived in the following sections.

Case I

The conditions for case I are the following:

1. 5 amperes $\leq I \leq$ 55 amperes
2. $360° F \leq T \leq T_{BPLO}$
3. Full regeneration ($\phi = 0$)
4. In-line heater off

To determine X for use in equation (96), the values of $\sum\left(\dot{m}C_p\right)_{cs}$ and $\sum\left(\dot{m}C_p\right)_{hs}$ are compared from equations (99) and (105), where in equation (105), $\phi = 0$.

At I = 5 amperes

$$\sum\left(\dot{m}C_p\right)_{cs} = 13.344 \text{ Btu/hr-°F} \tag{107}$$

and

$$\sum\left(\dot{m}C_p\right)_{hs} = 13.352 \text{ Btu/hr-}^\circ\text{F} \tag{108}$$

At I = 55 amperes

$$\sum\left(\dot{m}C_p\right)_{cs} = 13.786 \text{ Btu/hr-}^\circ\text{F} \tag{109}$$

and

$$\sum\left(\dot{m}C_p\right)_{hs} = 13.874 \text{ Btu/hr-}^\circ\text{F} \tag{110}$$

Therefore, $0.008 \leq \left[\sum\left(\dot{m}C_p\right)_{hs} - \sum\left(\dot{m}C_p\right)_{cs}\right] \leq 0.088$. It is evident from these calculations that the difference in hot-side and cold-side thermal capacity rates is always less than 0.1 Btu/hr-°F in the region of full regeneration, with $\sum\left(\dot{m}C_p\right)_{hs}$ only slightly greater than $\sum\left(\dot{m}C_p\right)_{cs}$. Therefore, it will be assumed that $\sum\left(\dot{m}C_p\right)_{hs} = \sum\left(\dot{m}C_p\right)_{cs}$; thus, the value of X is chosen to be $\sum\left(\dot{m}C_p\right)_{cs}$. The equation for cold-side regenerator effectiveness is then simplified considerably to

$$E_{cs} = \frac{T_s - T_R}{T - T_R} \tag{111}$$

By using a constant cold-side effectiveness of 0.84 in equation (111), the inlet temperature to the stack is

$$T_s = E_{cs}T + \left(1 - E_{cs}\right)T_R \tag{112}$$

By substituting equation (111) into equation (64) and denoting $Q_{recir\ out} - Q_{recir\ in}$ by Q_{recir}, the heat removed from the stack by the recirculation stream becomes

$$Q_{recir} = 13.3\left(1 - E_{cs}\right)\left(T - T_R\right) \tag{113}$$

To calculate the steady-state temperature of the fuel cell as a function of current, the steady-state heat balance is

$$Q = Q_{recir} + Q_{stack} \tag{114}$$

where Q is given by equation (69) with $\frac{dT}{dt} = 0$. Substituting equations (69), (42), and (113) into equation (114) gives

$$I(133.3 - 0.01043T - 3.413E) = \left[13.3\left(1 - E_{cs}\right)\left(T - T_R\right)\right] + (QA)T + B \tag{115}$$

where E is given by equation (71) (repeated here for convenience) as

$$E = (CAHI \cdot T + CBHI)I + (CDHI \cdot T + CEHI) - 0.2473\ (\text{percent } H_2O - 27.0) \tag{71}$$

As evidenced in appendix A (eq. (A6)), percent H_2O is given by

$$\text{percent } H_2O = 61.78 - 0.0997T + p_w \tag{116}$$

where p_w is the partial pressure of the water above the KOH, which is assumed here to be the equilibrium pressure calculated at the stack exit. From equation (56)

$$p_w = \frac{60}{1 + \frac{8.94}{\gamma}} \tag{56}$$

where γ is the specific humidity $\frac{lb_m\ H_2O}{lb_m\ dry\ H_2}$ of the mixture stream at the stack exit. By definition

$$\gamma = \frac{\dot{m}_{H_2O\ recir} + \dot{m}_{H_2O\ prod}}{\dot{m}_{H_2 recir}} \tag{117}$$

or

$$\gamma = \frac{2.70 + 22.98 \times 10^{-3} I}{3.51} \tag{118}$$

By substituting equation (56) into equation (116) and then substituting equation (116) into equation (71), the voltage relation (eq. (71)) becomes

$$E = [(CAHI)T + CBHI]I + [(CDHI)T + CEHI] + 0.02466T + \Gamma \tag{119}$$

where γ is given by equation (73), $\Gamma = \Gamma(I)$, and

$$\Gamma(I) = -8.601 - \frac{14.838}{1 + \frac{8.94}{\gamma}} \tag{120}$$

By substituting equation (119) into equation (115), simplifying, and then rearranging, the steady-state stack temperature T_{ss} becomes

$$T_{ss} = \frac{(-3.413 \cdot CBHI \cdot I^2) + [133.3 - (3.413 \cdot CEHI) - (3.413 \cdot \Gamma)]I + \left[13.3(1 - E_{cs})T_R\right] - QB}{(3.413 \cdot CAHI \cdot I^2) + [0.09459 + (3.413 \cdot CDHI)]I + \left[13.3(1 - E_{cs})\right] + QA} \tag{121}$$

This steady-state temperature will be used later as a boundary condition. The steady-state voltage for this case is given by equation (71) with $T = T_{ss}$. For the transient condition, by substituting equations (119) and (112) into the governing differential equation (eq. (70)), a linear first-order equation of the form of equation (75a) is obtained. However, the coefficients for this case are given by

$$A = 32 \tag{122}$$

$$B = (3.413CAHI)I^2 + (0.09459 + 3.413CDHI)I + 13.3 + QA - 13.3E_{cs} \tag{123}$$

$$C = (3.413CBHI)I^2 + (3.413CEHI + 3.413\ \Gamma - 133.3)I$$
$$+ QB - 13.3(1 - E_{cs})T_R \tag{124}$$

The temperature-time relationship for this case is the same as that of equation (82), where $T_{ss} = -\frac{C}{B}$.

Case II

The conditions for case II are as follows:

1. 5 amperes $\leq I \leq$ 55 amperes
2. $T_{BPLO} \leq T \leq T_{BPHI}$
3. Partial regneration
4. In-line heater off

Since $\sum(\dot{m}C_p)_{cs}$ and $\sum(\dot{m}C_p)_{hs}$ are approximately equal with full regeneration, it is evident that with any amount of regeneration $\sum(\dot{m}C_p)_{hs}$ will always be less than $\sum(\dot{m}C_p)_{cs}$. Therefore, $X = \sum(\dot{m}C_p)_{hs}$, and equation (96) becomes

$$E_{cs} = 0.84 = \frac{\sum(\dot{m}C_p)_{cs} \cdot (T_s - T_R)}{\sum(\dot{m}C_p)_{hs} \cdot (T - T_R)} \tag{125}$$

Now, the linear primary-bypass-valve characteristic (fig. 20) can be expressed mathematically as

$$\text{percent bypass} = (BP1 \cdot T) + BP2 \tag{126}$$

Typical bypass values of BP1 and BP2 are 2.167 percent/°F and -910.4 percent/°F, respectively, for $T_{BPLO} = 420°$ F.

By substituting equations (99), (105), and (126) into equation (125), simplifying, and solving for T_s, it is evident that

$$T_s = T_R + \beta_1 T^2 + \beta_2 T + \beta_3 \tag{127}$$

where

$$\beta_1 = \frac{-E_{cs} \cdot \alpha}{\sum(\dot{m}C_p)_{cs}} \left(BP1 \times 10^{-2}\right) \tag{128}$$

$$\beta_2 = \frac{E_{cs} \cdot \alpha}{\sum(\dot{m}C_p)_{cs}} \left[\left(1 - BP2 \times 10^{-2}\right) + \left(BP1 \times 10^{-2}\right)T_R\right] \tag{129}$$

$$\beta_3 = \frac{-E_{cs} \cdot \alpha \cdot T_R}{\sum(\dot{m}C_p)_{cs}} \left[1 - \left(BP2 \times 10^{-2}\right)\right] \tag{130}$$

By substituting equation (127) into equation (64)

$$Q_{recir} = \left(-13.3\beta_1\right)T^2 + \left[13.3\left(1 - \beta_2\right)T\right] - 13.3\left(T_R + \beta_3\right) \tag{131}$$

or

$$Q_{recir} = \delta_1 T^2 + \delta_2 T + \delta_3 \tag{132}$$

where $\delta_1 = -13.3\beta_1$, $\delta_2 = 13.3\left(1 - \beta_2\right)$, and $\delta_3 = -13.3\left(T_R + \beta_3\right)$. Again, the steady-state heat balance as given by equation (114) is

$$Q = Q_{recir} + Q_{stack} \tag{114}$$

Substituting equation (69), with $\frac{dT}{dt} = 0$, and equation (130) into equation (114) and then solving for the steady-state fuel-cell temperature T_{ss} gives

$$T_{ss} = \frac{-\xi_2 \pm \left(\xi_2^2 - 4\xi_1\xi_3\right)}{2\xi_1} \tag{133a}$$

where

$$\left.\begin{aligned} \xi_1 &= \delta_1 \\ \xi_2 &= (3.413 \cdot \mathrm{CAHI})I^2 + (3.413 \cdot \mathrm{CDHI} + 0.01043)I \\ &\quad + \delta_2 + \mathrm{QA} \\ \xi_3 &= (3.413 \cdot \mathrm{CBHI})I^2 + (3.413 \cdot \mathrm{CEHI} - 133.3)I \\ &\quad + \delta_3 + \mathrm{QB} \end{aligned}\right\} \tag{133b}$$

An order-of-magnitude analysis for the current region under consideration reveals that the positive root must be chosen in equation (133a) for T_{ss} to make the mathematical model compatible with the actual fuel cell. Therefore

$$T_{ss} = \frac{-\xi_2 + \sqrt{\xi_2^2 - 4\xi_1\xi_3}}{2\xi_1} \tag{134}$$

The order-of-magnitude analysis also insures that for the current region considered the discriminant $\xi_2^2 - 4\xi_1\xi_3$ is always greater than zero, thereby avoiding the possibility of imaginary roots.

By using equation (71) in conjunction with equation (134), the steady-state voltage for this case can be obtained. The differential equation for the transient condition is derived by substituting equations (119) and (127) for E and T_s, respectively, into

equation (70). This yields

$$32\frac{dT}{dt} + \delta_1 T^2 + (\delta_2 - \delta_4)T - C_1 = 0 \tag{135}$$

where

$$\delta_4 = -(3.413 \cdot CAHI)I^2 - (3.413 \cdot CDHI + 0.01043)I - QA \tag{136}$$

and

$$C_1 = -(3.413 \cdot CBHI)I^2 - (3.413 \cdot CEHI - 133.3)I - \delta_3 - QB \tag{137}$$

Note that for steady-state conditions $\left(\frac{dT}{dt} \rightarrow 0\right)$, the constant C_1 can also be evaluated as

$$C_1 = \delta_1 T_{ss}^2 + (\delta_2 - \delta_4)T_{ss} \tag{138}$$

where T_{ss} is given in equation (134).

Equation (135) can be rearranged and integrated as

$$\int_{T_1}^{T} \frac{32\,dT}{a + bT + cT^2} = \int_{t_0}^{t} dt \tag{139}$$

where $a = C_1$, $b = (\delta_4 - \delta_2)$, and $c = -\delta_1$. Now, by defining q as $4ac - b^2$, the value of the stack temperature at any time after a step load change from I_1 to I_2 (where the stack temperature was T_1 at t_0 when the load changed instantaneously) is

$$T = -\frac{b}{2c} + \left(\frac{\sqrt{q}}{2c}\right)\left\{\tan\left[\tan^{-1}\left(\frac{2cT_1 + b}{q}\right) + \frac{\sqrt{q}}{64}(t - t_0)\right]\right\} \tag{140}$$

for $q > 0$, and

$$T = -\frac{b}{2c} + \left(\frac{\sqrt{-q}}{2c}\right)\left\{\tanh\left[\tanh^{-1}\left(\frac{2cT_1 + b}{-q}\right) - \frac{\sqrt{-q}}{64}(t - t_0)\right]\right\} \tag{141}$$

for $q < 0$, where the positive root is always used for $\sqrt{q}$ and $\sqrt{-q}$.

The voltage at any temperature T is given by equation (71).

Case III

The conditions for case III are as follows:

1. 5 amperes $\leq I \leq$ 55 amperes
2. 360° F $\leq T \leq 420^\circ$ F
3. Full regeneration ($\phi = 0$)
4. In-line heater on

Although the equations for this case are good for 360° F $\leq T \leq 420^\circ$ F, the in-line heater is designed to sense stack temperature, so that if the stack temperature is falling the heater is activated when the temperature reaches some temperature T_{low} in the range of $380^\circ \pm 5^\circ$ F. The heater then stays on until the stack temperature has risen to some temperature T_{high} in the range of $390^\circ \pm 5^\circ$ F. The actual values of T_{low} and T_{high} vary from power plant to power plant. The in-line heater dumps heat into the power plant for low-power operation according to the equation

$$Q_{htr} = \frac{3.413E^2}{R_{htr}} \tag{142}$$

Since the voltage varies only slightly within the relatively narrow temperature dead band (only 3° or 4° on most power plants) in which the heater is on, a constant heater power based on 31 volts will be used in the analysis. Heater resistance is 6.02 ohms. By substituting these values into equation (142), the heater power is found to be 159.6 watts, or 544.8 Btu/hr. It is assumed that all of this heat is used in raising the temperature of the power plant. For the purpose of calculating a steady-state temperature with the heater on, equation (36) becomes

$$Q + Q_{htr} = Q_{stack} + Q_{recir} \tag{143}$$

By using the voltage equation (eq. (119)) in conjunction with (1) equation (140) for Q (with $\frac{dT}{dt} = 0$), (2) equation (113) for Q_{recir}, (3) $Q_{stack} = (QA \cdot T) + QB$, and (4) $Q_{htr} = 544.8$ Btu/hr, the steady-state stack temperature with the heater on is given by

$$T_{ss} = \frac{13.3(1 - E_{cs})T_R + 544.8 - QB + 133.3I_{tot}\left[(CBHI \cdot I_{tot}) + CEHI + \Gamma\right]}{13.3(1 - E_{cs}) + 0.01043I_{tot} + 3.413I_{tot}\left[(CAHI \cdot I_{tot}) + CDHI + 0.02466\right] + QA} \tag{144}$$

where Γ is calculated on the basis of total current I_{tot}, and $I_{tot} = I + I_{htr} = I + 31/6.02$, or

$$I_{tot} = I + 5.15 \tag{145}$$

The transient equation for this case is the same as equation (82) in case I, except that the steady-state temperature T_{ss} is the same as in equation (144).

Case IV

The conditions for case IV are as follows:

1. $0 \leq I \leq 5$ amperes
2. $T_{high} \leq T \leq T_{BPLO}$
3. Full regeneration ($\phi = 0$)
4. In-line heater off

To calculate T_{ss} for case IV, equation (72) is modified by substituting equation (56) into equation (116) and then substituting equation (116) into equation (72) to obtain

$$E = [(CALO \cdot T) + CBLO]I + (CDLO + 0.0247)T + \Gamma \tag{146}$$

where $\Gamma = -8.601 - \frac{14.838}{1 + \frac{8.94}{\gamma}}$.

For case IV, the steady-state temperature, obtained by substituting equation (146) into equation (115), is

$$T_{ss} = \frac{(-3.413CBLO)I^2 + (133.3 - 3.413CELO - 3.413\Gamma)I + 13.3(1 - E_{cs})T_R - QB}{(3.413CALO)I^2 + (0.09459 + 3.413CDLO)I + 13.3(1 - E_{cs}) + QA} \tag{147}$$

For the transient condition, by substituting equations (146) and (112) into equation (70), the governing equation takes the form of equation (75a) with the constants A, B, and C given by equations (122), (123), and (124); however, in equations (121), (122), and (123) the voltage curve fit constants CAHI, CBHI, CDHI, and CEHI are replaced by CALO, CBLO, CDLO, and CELO, respectively. The value of Γ for case IV is the same as in equation (146). The solution to the differential equation is given by equation (82), with the value of T_{ss} the same as in equation (147).

Case V

The conditions for case V are as follows:

1. $0 \leq I \leq 5$ amperes
2. $T_{BPLO} \leq T \leq T_{BPHI}$
3. Partial regeneration ($\phi \neq 0$)
4. In-line heater off

For case V, the only three parameters which are different from case II are ξ_2, ξ_3, and δ_4. These are derived using the same techniques as were used in case II, except that equation (146) is used for the voltage instead of equation (119). The equations for ξ_2, ξ_3, and δ_4 are

$$\xi_2 = (3.413CBLO)I^2 + (3.413CDLO + 0.01043)I + \delta_2 + QA \tag{148}$$

$$\xi_3 = (3.413CBLO)I^2 + (3.413CELO - 133.3)I + \delta_3 + QB \tag{149}$$

$$\delta_4 = -(3.413CALO)I^2 - (3.413CDLO + 0.01043)I - QA \tag{150}$$

and the value of Γ is the same as that used in equation (146). The steady-state and transient temperature equations are the same as for case II, except that the new values of ξ_2, ξ_3, and Γ are used for case V.

The foregoing equations were used to formulate a computer program which accepts a given current profile and predicts the thermal response of the fuel cell to the demand load imposed upon it. The computer program is described in appendix B. A computer program was also written for the simplified analysis presented in the section on simplified transient analysis.

COMPARISON OF ANALYTICAL RESULTS

Before comparing the results of the general analysis to the test data obtained in the thermal vacuum chamber, the results of the simplified analysis and the general analysis will be compared. Figure 21 illustrates this comparison for a sample current profile. It is evident from the figure that the incorporation of the primary regenerator and the bypass valve into the analysis, which is the major difference between the simplified and general analyses, has two main effects. First, by using the equations of the general analysis, the thermal response time of the fuel cell is much smaller in the region of regeneration than the response time obtained from the simplified analysis. Second, by using the equations of the general analysis, the operating-temperature range of the fuel cell is narrowed considerably, particularly at high-power loads.

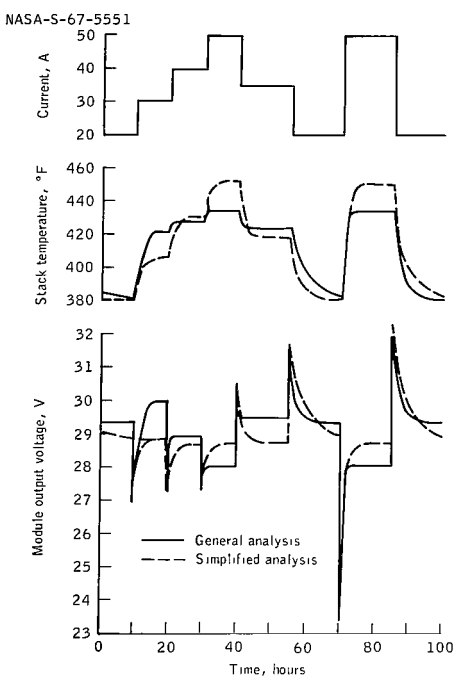

Figure 21. - Comparison of results of the simplified analysis and the general analysis.

The steady-state voltage-current characteristic of the fuel-cell module (obtained by using the equations of the general analysis) is compared in figure 22 to the thermal-vacuum characteristics (obtained from test data taken from in-house performance evaluations of Apollo fuel-cell power systems) of two qualified Apollo fuel-cell modules. The steady-state voltage-current characteristic obtained with the simplified analysis is also included for comparison. In this figure, the large error incurred by use of the simplified analysis is shown clearly. As is evident in the figure, the general analysis gives a more realistic approximation to actual fuel-cell performance.

The empirical data used in the equations are a statistical average of data obtained from many actual power plants and components. Because each power plant is a separate entity, the performance of

each will be slightly different. Therefore, the mathematical model can only be expected to predict average power plant performance. Examples of performance differences between actual power plants are indicated by variations in the steady-state voltage-current characteristic (fig. 22).

The discontinuity in the characteristic curves (fig. 22) of the general analysis and the qualified power plants is that point at which the primary bypass valve is fully closed and the power plant is in a condition of full regeneration. If the current is further decreased from this point, no more regeneration is obtained, and the stack temperature settles to a lower steady-state value, thereby lowering the steady-state voltage.

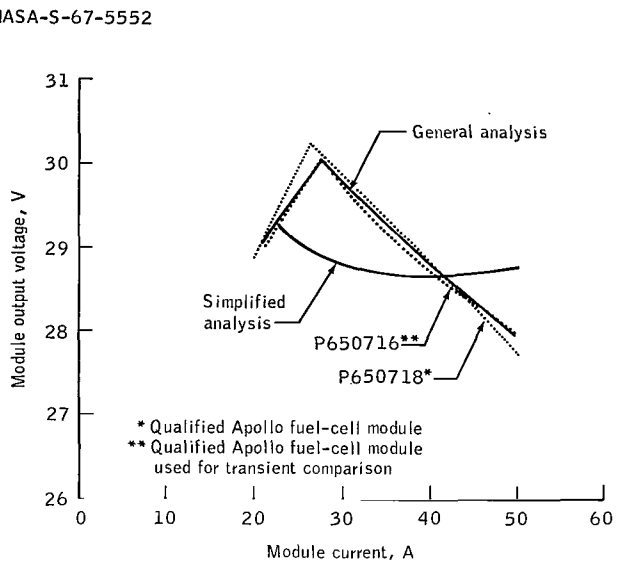

Figure 22. - Comparison of steady-state voltage current characteristics.

The constant-temperature lines shown in the voltage-current plot in figure A-1 of appendix A for a constant electrolyte (H_2O) concentration of 27 percent are not included in figure 22 because at each different point on the steady-state characteristic line, the electrolyte concentration has a different value. If lines of constant temperature and constant concentration were both shown, a three-dimensional plot would be needed.

In figures 23(a) to 23(d), the transient performance results of the general analysis are compared to actual test data obtained for various step load changes from in-house performance evaluations of a qualified Apollo fuel-cell module. Note in making the comparison, that the steady-state voltage values of the general analysis will be slightly higher in the regeneration region than those of the qualified power plant to which they are compared in figure 22. At low currents, however, the two steady-state lines approach each other.

In the figures, the glycol-coolant inlet temperature to the module and the glycol flow rate through the condenser are given for the test module. These two quantities determine the primary-side condenser exit temperature $T_{c/e}$ for any given fuel-cell load. The maximum and minimum values of $T_{c/e}$ observed during the various test sequences are also shown on the figures for comparison with the constant condenser exit temperature of 160° F assumed in the general analysis. The variations in condenser exit temperature are partially caused by the fact that as fuel-cell load increases more water is produced, with a resultant increase in the partial pressure of the water vapor in the primary loop and a consequent increase in condenser exit temperature.

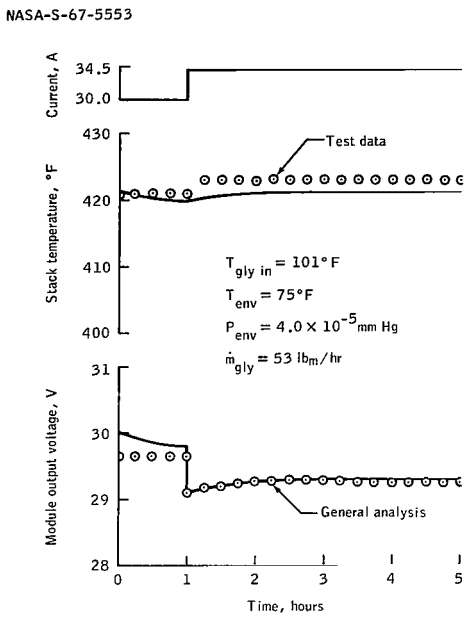

(a) 159.9° F ≤ $T_{c/e}$ ≤ 166.3° F.

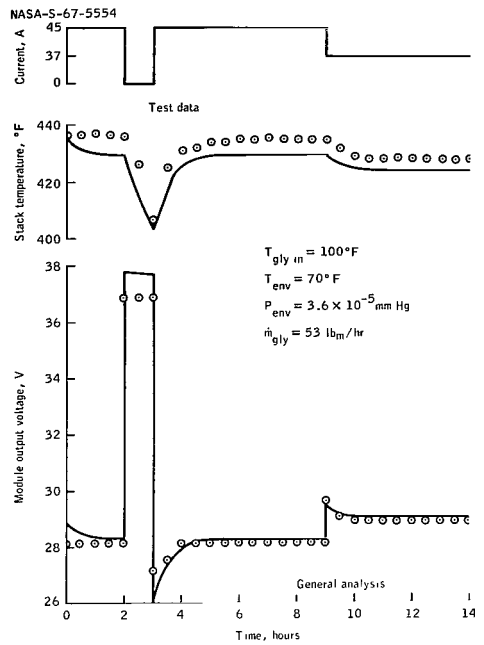

(b) 157.0° F ≤ $T_{c/e}$ ≤ 167.1° F.

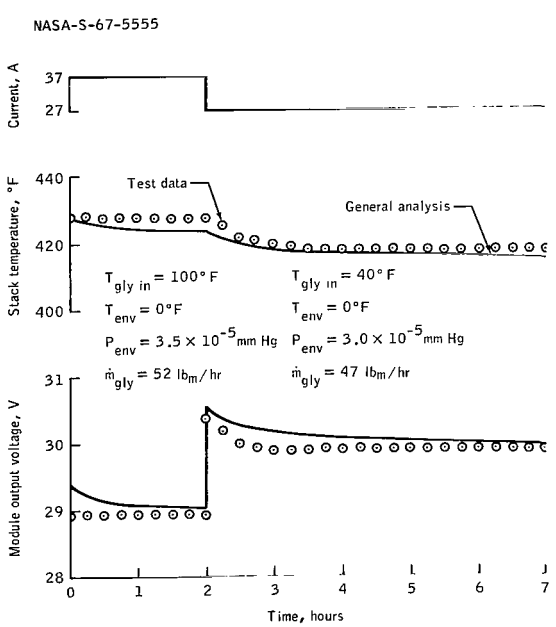

(c) 158.0° F ≤ $T_{c/e}$ ≤ 165.5° F.

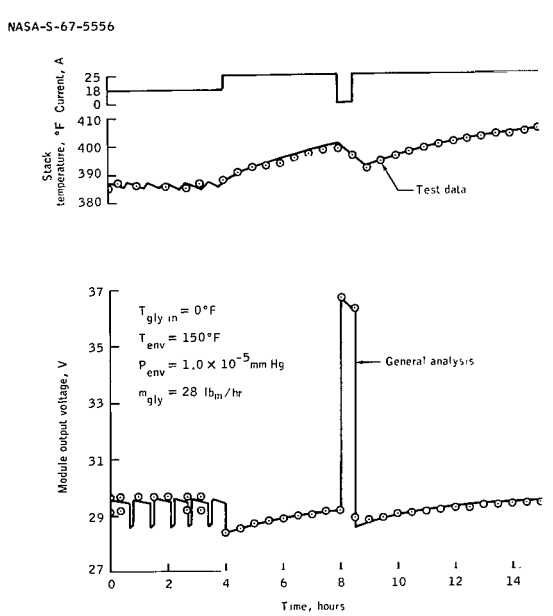

(d) 159.5° F ≤ $T_{c/e}$ ≤ 164.5° F.

Figure 23. - Comparison of results of general analysis with vacuum-chamber test data.

Figure 23(a) indicates a step from 30.0 to 34.5 amperes with condenser exit temperature varying between 159.9° and 166.3° F on the test module. The steady-state voltage of the test module is approximately 0.1 volt lower than that of the analytical model, while the steady-state temperature of the test module is higher than that of the analytical model by about 5° F. As illustrated in figure 23(b), the stack temperature was allowed to settle for 2 hours at 45 amperes; then the power plant was put on open circuit. The analytical model and the test module compared favorably in temperature just before the load was increased to 45 amperes. Six hours later, the load was decreased to 37 amperes. This also is illustrated in figure 23(b). Note that figure 23(c) also illustrates the temperature and voltage response comparison for a step load decrease in current.

The first part of figure 23(d) illustrates the operation of the low-power in-line heater. The temperature dead band of the analytical model was set between 385° and 387° F and thus compared favorably with the test module. Note, however, that the voltage drop in the analytical model when the heater is energized exceeds that of the test module. This is caused partly by the use of a smaller heating-element resistance in the analytical model, which causes the model to draw a larger heater current at some nominal voltage and results in a larger voltage drop. The larger voltage drop in the analytical model is also caused by the selection of a nominal module voltage of 31 volts (assumed constant) when the in-line heater is energized. The in-line heater of the analytical model was energized more frequently than that of the test module because the fuel-cell environment temperature of the test module was 150° F; whereas, an environment temperature of 77° F was used in the general analysis. This increased environment temperature of the test module caused a lower stack heat loss than the environment temperature used in the general analysis.

Figure 23(d) illustrates a very interesting feature of the general analysis. When the load is increased from 18 to 25 amperes at $t = 4$ hours, the stack temperature for the analytical model has just dropped to 385° F, which causes the heaters to be energized with simultaneous application of the step load. This results in a total instantaneous current demand of 12.15 amperes (since for the analytical model the heater current is assumed constant at 5.15 amperes), thus causing a voltage drop to 27.1 volts. In the test module, however, the in-line heater was still off when the step load was applied, and thus the voltage only dropped to 28.6 volts. Several minutes after $t = 4$ hours, the stack temperature of the analytical model reached 387° F, which caused the heater to be deenergized and the voltage to rise instantaneously to 28.55 volts, from which point the normal transient voltage buildup continued. At $t = 8$ hours, the power plant was put on open circuit for 31 minutes. After this time, the 25-ampere load was resumed.

CONCLUDING REMARKS

From the steady-state voltage-current-characteristic comparison, it is evident that the general analysis yields a characteristic curve which compares favorably with the curve for the qualified Apollo fuel-cell module used for transient comparison. The comparison of the transient response of the general analysis to the response of the qualified fuel-cell module yields the conclusion that the equations derived in the general analysis and the representative performance characteristics which served as inputs to the

analysis are adequate to describe the performance of an actual fuel-cell system throughout its normal operating range for both the steady-state and the transient modes of operation.

The following is a summary of the principal limitations of the analysis.

1. The predicted values of the analysis are only valid for a fuel-cell power plant operating in a vacuum environment.

2. The analysis is restricted to a normal range of glycol-coolant inlet temperatures such that the condenser exit temperature on the primary side remains within approximately ±10° from 160° F.

3. The environment temperature of the fuel cell is restricted to temperatures in the region of 77° F. It is thought that a variation of ±20° F from 77° F would be tolerable.

4. The stack heat loss is assumed to have only a linear variation with temperature. Little is known about the stack heat loss, since the stack and the primary regenerator are inside the pressure vessel where it is very difficult to place instrumentation. However, it is thought, and test-data comparisons seem to agree, that the linear assumption is adequate for a temperature of 77° F.

5. The cold-side effectiveness of the primary regenerator was assumed to be constant at 84 percent. (Cold-side effectiveness is known to be a function of temperature, percent bypass, and specific humidity.) This limitation and limitation 4 do not appear to cause serious errors in the computations, however.

6. By assuming a purely resistive load, Ohm's law dictates that the current through the load is a function of the voltage impressed upon it which, in the actual spacecraft, is fuel-cell output voltage. However, the fuel-cell output voltage changes with fuel-cell temperature, fuel-cell concentration, and other variables, as observed in the analysis, which causes fluctuations in fuel-cell output current. Although these fluctuations are usually small, this effect should be taken into account. This was not done in this analysis.

In conclusion, it is believed that this analysis presents an adequate mathematical model for predicting fuel-cell performance, subject to the limitations imposed upon the study. If performance predictions are desired for power plants other than the fuel-cell used for transient comparison, the performance characteristics of the specific power plant under consideration must serve as an input to the computer program.

Areas of further study in order of priority are as follows:

1. Taking the effects of variable current into consideration would mean an iterative-type solution in which, at any given time, a fuel-cell output voltage is assumed for a given resistance input. From this assumption a current is calculated. By using this current as an input to the general analysis, fuel-cell temperature and voltage are calculated for the given time. The calculated voltage is compared to the assumed voltage. If the two are not equal, some new voltage is assumed, and the process is

repeated until the calculated and assumed voltages are within a reasonable tolerance. The computation then proceeds to the next time step, and the whole iteration process is repeated.

2. Taking into account the variations of fuel-cell performance with changes in environment temperature would include trying to define the stack heat loss more accurately, since stack heat loss is a function of environment temperature and stack temperature.

3. The effect of voltage degradation with time caused by the buildup of impurities within the cells is another area of further study.

4. Taking into account the variations in fuel-cell performance caused by changes in condenser exit temperature on the primary side would entail an analysis of condenser and secondary-loop performance.

The analytical techniques required to formulate a mathematical model for a complex system such as the fuel-cell system may at first appear to be unique and, therefore, lacking in general applicability; however, there is a common body of knowledge in modeling and simulation which is broadly applicable and of great help to the systems engineer. This report is only one application of these general techniques, but the approach taken and the methods used are sufficiently general to allow application to other types of systems.

Manned Spacecraft Center
National Aeronautics and Space Administration
Houston, Texas, January 12, 1968
941-13-05-01-72

APPENDIX A

DEVELOPMENT OF EMPIRICAL RELATION FOR FUEL-CELL POWER PLANT OUTPUT VOLTAGE AS A FUNCTION OF CURRENT, TEMPERATURE, AND ELECTROLYTE CONCENTRATION

To obtain the necessary relation for the module output voltage, a statistical compilation of test data (triangular points) taken from many power plants is plotted (fig. A-1). Test data are not readily available for the open-circuit condition at temperatures above 440° F or for the current region between open circuit and approximately 15 amperes. Therefore, values in this region can only be estimated. The comparison in figure A-1 is made for a constant electrolyte concentration of 27 percent water by weight.

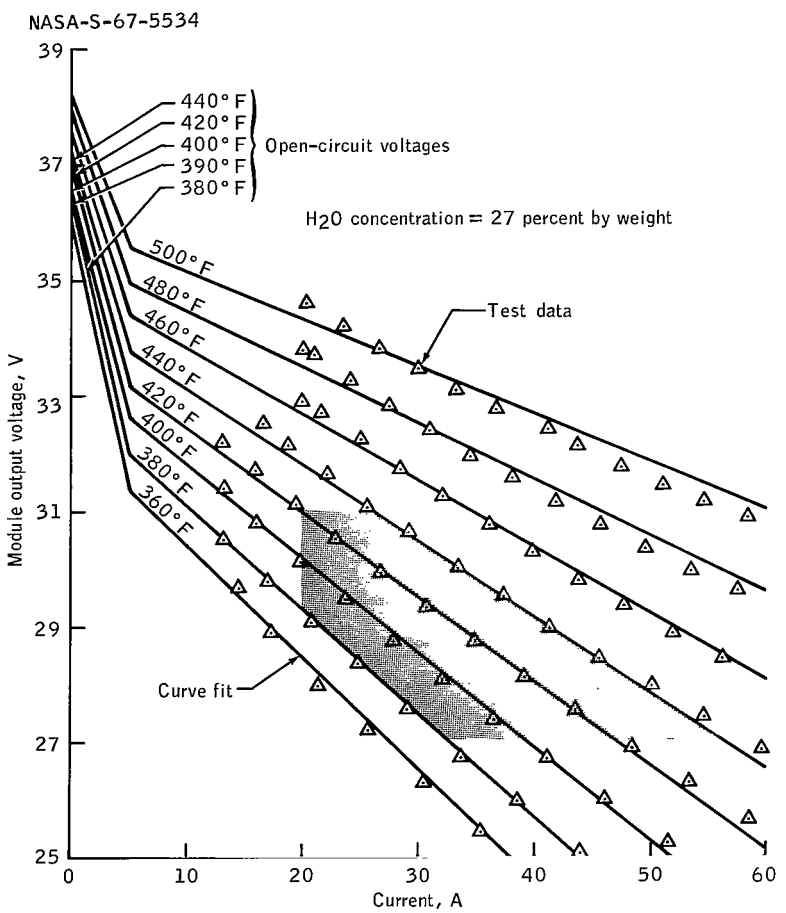

Figure A-1. - Comparison of polarization curves of analytical model with those of statistical test data.

Since the fuel cell normally operates at temperatures between 380° and 440° F, at currents between 20 and 55 amperes, and at voltages between 27 and 31 volts, only the data points in the shaded area in figure A-1 were considered for the current region from 5 to 55 amperes. From these points, it is evident that at any specified temperature, the module output voltage is essentially a linear function of current. The voltage equation would thus have the form

$$E = m_1 I + b_1 \tag{A1}$$

where m_1 is the slope, and b_1 is the Y-intercept.

By assuming linearity, the slope and the Y-intercept are calculated for each constant-temperature line between 380° and 440° F. Figure A-2 is a plot of m_1 versus T and b_1 versus T. Calculations indicate that the use of a first-order approximation in the most-frequented operating-temperature range (400° to 440° F) produces only a very small error in the voltage calculation for the region between 380° and 400° F. This approximation yields relations for the slope and Y-intercept as a function of temperature as follows.

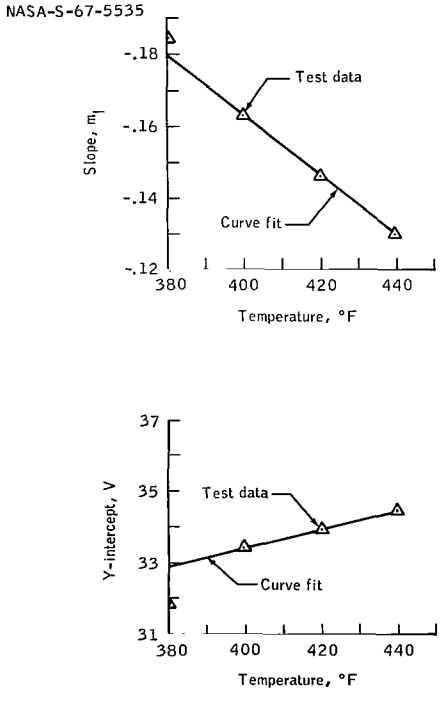

Figure A-2. - Variation of slope and Y-intercept of constant-temperature voltage lines with temperature.

$$m_1 = 7.96 \times 10^{-4} T - 0.481 \tag{A2}$$

$$b_1 = 0.026T + 23.0 \tag{A3}$$

By substituting equations (A2) and (A3) into equation (A1), the voltage variation E_v with current and temperature at a constant electrolyte concentration of 27 percent water is

$$E_v = \left(7.96 \times 10^{-4} T - 0.481\right) I + (0.026T + 23.0) \tag{A4}$$

where 5 amperes $\leq I \leq$ 55 amperes, and 380° F $\leq T \leq$ 440° F.

It is evident in figure A-1 that agreement between the test data and equation (A4)

is very good within the region considered. There is also good agreement considerably outside of this region.

To account for changes in electrolyte concentration, a correction factor K_c is introduced. Thus, the general voltage equation can be written as

$$E = E_v + K_c \text{ (percent } H_2O - 27.0) \tag{A5}$$

Extensive tests conducted on single cells, on six-cell stacks, and on complete modules have shown that K_c is essentially constant over the normal electrolyte-concentration operating range of the fuel cell, which is less than ± 2 percent H_2O about the nominal 27 percent H_2O. The value of K_c from these tests is -0.2473 V/Δ percent H_2O above 27 percent. Thus, the general equation for the variation of module output voltage with current, temperature, and electrolyte concentration is

$$E = \left(7.96 \times 10^{-4}T - 0.481\right)I + (0.026T + 23.0) - 0.2473 \text{ (percent } H_2O - 27.0) \tag{A6}$$

where 5 amperes $\leq I \leq$ 55 amperes, 380° F $\leq T \leq$ 440° F, and 22 $\leq$ percent $H_2O \leq$ 32. It is evident from equation (A6) that an increase in fuel-cell operating (stack) temperature will raise the voltage output of the module correspondingly. For the temperature range considered, the term $7.96 \times 10^{-4}T - 0.481$ is always negative; therefore, a current increase causes a decrease in module output voltage.

The quantity percent H_2O is calculated using the assumption of equilibrium for the partial pressure of the water vapor above the KOH within the stack. Under this assumption, the electrolyte concentration is a function of (1) the partial pressure of the water above the KOH and (2) the temperature. Figure A-3 is a plot of a statistical average for percent KOH as a function of these two variables taken from actual laboratory data (triangles). For a nominal fuel-cell condenser exit temperature of 160° F on the primary side, the partial pressure of the water above the KOH will always be between 4.6 and 7.0 psia. A first-order approximation biased to the most-frequented region is again used. Figure A-4 is a plot of the variations of slope and Y-intercept. The slope is approximately constant at -1.0 percent change in KOH per unit change in partial pressure. By using a straight line fit for the Y-intercept in figure A-4, the relationship

NASA-S-67-5536

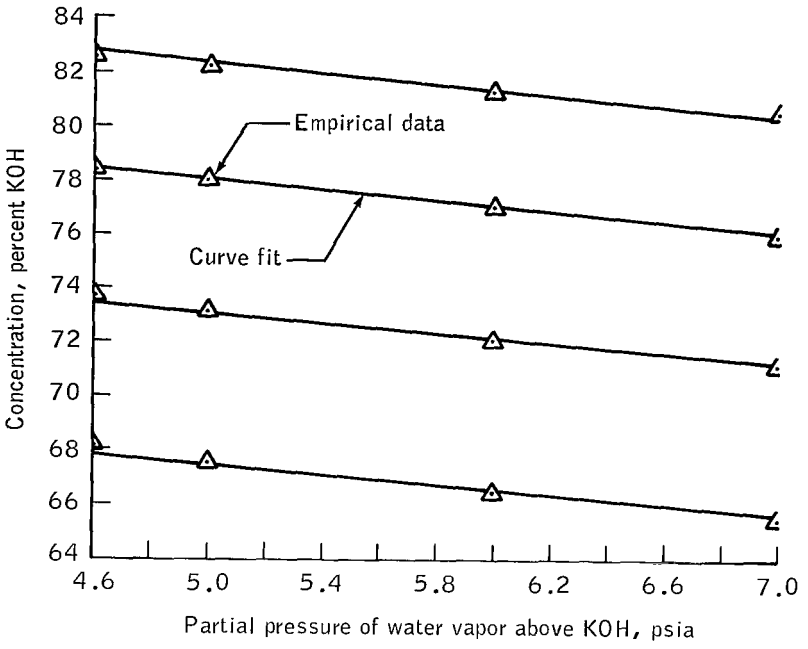

Figure A-3. - Variation of electrolyte concentration with temperature and partial pressure.

NASA-S-67-5539

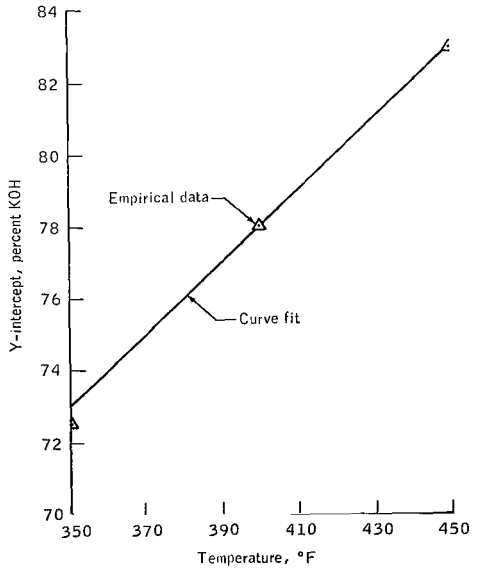

Figure A-4. - Variation of Y-intercept of constant-temperature concentration lines with temperature.

for electrolyte concentration as a function of partial pressure and temperature is percent KOH = 0.0997T + 38.22 - p_w, from which

$$\text{percent } H_2O = 61.78 - 0.0997T + p_w \tag{A7}$$

where 350° F ≤ T ≤ 500° F, and 4.6 psia ≤ p_w ≤ 7.0 psia. Equation (A7) is used in conjunction with equation (A6) in the analysis.

Since very little data could be obtained for this analysis between open circuit and 20 amperes, the linear fit in equation (A4) is used down to 5 amperes. Then, using test-data values for open-circuit voltage, the same procedure used in the derivation of equation (A4) is used for the low-current region (0 to 5 amperes), with the result that

$$E = \left(2.775 \times 10^{-3}T - 1.903\right)I + (0.0157T + 30.24) - 0.2473\ (\text{percent } H_2O - 27.0) \tag{A8}$$

where the same correction factor used before for concentration changes is applied. Percent H_2O is calculated from equation (A7), the limits of which are sufficient to include operation down to open-circuit conditions. The solid lines in figure A-1 are a plot of E from equation (A8) for various temperatures.

Equations (A6) and (A8) represent the empirical relations used in the analysis for the high-current (5 to 55 amperes) and low-current (0 to 5 amperes) regions, respectively. These two equations should be used with equation (A7) for percent H_2O. The quantity p_w is calculated from equation (56).

APPENDIX B

THE COMPUTER PROGRAM FOR THE GENERAL ANALYSIS

A digital computer program was written for the simplified analysis presented in the section on simplified transient analysis and was later expanded for the general analysis presented in the section on general transient analysis. The program for the general analysis is presented in this appendix.

The digital program accepts a current-time profile and predicts for this profile the transient temperature and voltage response of the fuel-cell module. The program includes the five current and temperature regions of operation for which transient equations were developed in the section on general transient analysis.

SYMBOLS

A	collection of terms used in the equations for simplification
AGAMA	collection of terms used in the equation for simplification. AGAMA is a function of GAMA, and is denoted by Γ in the analysis
B	collection of terms used in the equations for simplification
BP	percent bypass around primary regenerator
BP1, BP2	curve fit constants for primary-bypass-valve characteristic
C	collection of terms used in the equations for simplification
C1	collection of terms used in the equations for simplification
CAHI, CBHI, CDHI, CEHI	curve fit constants for fuel-cell performance characteristics in the high-current region, $5 \text{ A} \leq I \leq 55 \text{ A}$
CALO, CBLO, CDLO, CELO	curve fit constants for fuel-cell performance characteristics in the low-current region, $0 \leq I \leq 5 \text{ A}$
COLD	$\sum(\dot{m}C_p)_{cs}$ for hydrogen and water vapor at cold side to primary regenerator, Btu/° F

DELHT	length of time the in-line heater stays on, hr
DISCRM	discriminant of the polynomial in W_1, W_2, and W_3
DT	time increment for transient temperature and voltage calculations, hr
DT1	dummy variable (time) increment used in calculating the time at which the bypass valve closes, hr
E	module voltage, V
EPR	primary regenerator cold-side effectiveness (fractional)
ESS	steady-state module voltage, V
G	dummy variable, equal to $\sqrt{q}$ or $\sqrt{-q}$, depending on whether q is positive or negative
GAMA	specific humidity of hydrogen and water-vapor mixture at stack outlet, $\frac{lb_m\ H_2O}{lb_m\ dry\ H_2}$
HTIME	time index used to calculate the length of time the in-line heater stays on, hr
I	total fuel-cell current after a given step load change $(I = I_2 + I_{htr})$, A
I1	current before step load change, A
I2	current after step load change, A
IHTR	current drawn by in-line (low-power) heater, A
LAMBDA	time constant for fuel-cell transient response, hr^{-1}
PCH20	percent H_2O in electrolyte solution
PSS	steady-state power level, W
PW	partial pressure of water vapor at stack outlet, psia
Q	negative discriminant of polynomial in A, B, and C
QA, QB	curve fit constants for stack heat loss
RT	variable time used to calculate the transient temperature and voltage values between TIME1 and TIME2, hr

RT1	dummy variable (time) used in calculating the time at which the bypass valve closes, hr
S	time index used in calculating the time at which the primary bypass valve closes, hr
T	fuel-cell (stack) temperature at any time, °F
T1	initial fuel-cell temperature at each step load change, °F
TAN	collection of terms used in the equations for simplification
TB	dummy variable (temperature)
TBPHI	temperature of bypass, high
TBPLO	temperature of bypass, low
THETA, THETA1, THETA2	collection of terms used in the equations for simplification
THOF	temperature at which the in-line heater is deenergized, °F
THON	temperature at which the in-line heater is energized, °F
TIME	dummy variable used in calculating the time at which the primary bypass valve opens, hr
TIME1	dummy variable used to initialize time at each step load change, hr
TIME2	time at which the load changes from I2 (or I, if in-line heater is on) to some new value of current (I2 equals fuel-cell current from TIME1 to TIME2), hr
TO	initial time of current I2 (or I, if in-line heater is on) (TO = TIME1), hr
TR	temperature of hydrogen and water-vapor mixture at cold-side inlet of primary regenerator, °F
TSS	steady-state fuel-cell (stack) temperature, °F
TSTART	initial temperature of fuel-cell stack at time t = 0, °F
W1, W2, W3	collection of terms used in the equations for simplification; denoted by ξ_1, ξ_2, and ξ_3 in the analysis

X1, X2, X3, X4	collection of terms used in the equations for simplification
Y1, Y2, Y3	collection of terms used in the equations for simplification; denoted by β_1, β_2, and β_3 in the analysis
Z	term used in the equations for simplification; denoted by α in the analysis
Z1, Z2, Z3, Z4	collection of terms used in the equations for simplification; denoted by δ_1, δ_2, δ_3, and δ_4 in the analysis

```
      PROGRAM MAIN
      REAL I1,I2,IHTR,I,LAMBDA
      WRITE(6,1)
    1 FORMAT(55H1TRANSIENT THERMODYNAMIC ANALYSIS OF A FUEL CELL SY
     17H SIMON //)
   50 READ(5,51) CAHI,CBHI,CDHI,CEHI,CALO,CBLO,CDLO,CELO
   51 FORMAT(8F10.0)
      IF(CAHI.EQ.0.0) GO TO 2000
      READ(5,51)BP1,BP2,TBPLO,TBPHI
      READ(5,9)EPR
      READ(5,51)QA,QB
      READ(5,51)THON,THOF
   70 READ(5,9) DT
      READ(5,9)TSTART
    9 FORMAT(F10.0)
      TIME1=0.0
      T1=TSTART
      T=T1
    5 READ(5,10) TIME2,I2
   10 FORMAT(2F10.0)
      IF(TIME2)50,70,80
   80 WRITE(6,999)
      T0=TIME1
      RT=T0
    2 IF(T.LT.350.) GO TO 24
      TR=(0.681*I2+2261.)/(8.841E-03*I2+13.3)
      GAMA=(2.70+22.976E-03*I2)/3.51
      PW=60.0/(1.0+8.94/GAMA)
      AGAMA=-8.601-14.838/(1.0+8.94/GAMA)
      IF(T.LE.TBPLO) GO TO 3
      IHTR=0.0
   17 IF(T.GT.TBPHI)GO TO 4
      COLD=8.841E-03*I2+13.3
      Z=10.431E-03*I2+13.3
      Y1=-EPR*Z*BP1*.01/COLD
      Y2=(EPR*Z/COLD)*(1.0-BP2*.01+BP1*TR*.01)
      Y3=(EPR*Z*TR/COLD)*(BP2*.01-1.0)
      Z1=-13.3*Y1
      Z2=13.3*(1.0-Y2)
      Z3=-13.3*(TR+Y3)
      W1=Z1
      IF(I2.LT.5.0) GO TO 34
      W2=Z2+0.08416*I2+3.413*I2*CDHI+3.413*I2**2*CAHI+0.01043*I2+QA
      W3=Z3        +3.413*I2*AGAMA+3.413*I2*CEHI+3.413*I2**2*CBHI-13.
     12+QB
   28 DISCRM=W2**2-4.0*W1*W3
      IF(DISCRM.LT.0.0) GO TO 20
      TSS=(-W2+SQRT(DISCRM))/(2.0*W1)
      PCH2O=61.78-0.0997*TSS+PW
      IF(I2.LT.5.0) GO TO 38
      ESS=(CAHI*TSS+CBHI)*I2+(CDHI*TSS+CEHI)-0.2473*(PCH2O-27.0)
      GO TO 39
   38 ESS=(CALO*TSS+CBLO)*I2+(CDLO*TSS+CELO)-0.2473*(PCH2O-27.0)
   39 IF(I2.GE.5.0) GO TO 35
      Z4=-3.413*CALO*I2**2+(-3.413*CDLO-0.01043-0.08416)*I2
      GO TO 29
```

```
   35 Z4=-3.413*CAHI*I2**2+(-3.413*CDHI-0.01043-0.08416)*I2
   29 C1=Z1*TSS**2+(Z2-Z4+QA)*TSS
      A=C1
      B=Z4-Z2-QA
      C=-Z1
      Q=4.0*A*C-B**2
      IF(Q)6,7,8
    6 G=SQRT(-Q)
      X1=(2.0*C*T1+B)/G
   14 X2=-TANH((G*(RT-T0))/64.0)
      T=-B/(2.0*C)+(G/(2.0*C))*((X1+X2)/(1.0+X1*X2))
      PCH2O=61.78-0.0997*T+PW
      IF(I2.LT.5.0) GO TO 40
      E=(CAHI*T+CBHI)*I2+(CDHI*T+CEHI)-0.2473*(PCH2O-27.0)
      GO TO 11
   40 E=(CALO*T+CBLO)*I2+(CDLO*T+CELO)-0.2473*(PCH2O-27.0)
   11 IF(T.GT.TBPHI)GO TO 4
      IF(T.LE.TBPLO)GO TO 12
      BP=BP1*T+BP2
      WRITE(6,1000)RT,I2,E,T,BP,PCH2O,IHTR
      IF(RT.GE.TIME2)GO TO 60
      RT=RT+DT
      GO TO 14
   34 W2=Z2+0.08416*I2+3.413*I2*CDLO+3.413*I2**2*CALO+0.01043*I2+QA
      W3=Z3       +3.413*I2*AGAMA+3.413*I2*CELO+3.413*I2**2*CBLO-13.
     12+QB
      GO TO 28
    4 WRITE(6,2001)
 2001 FORMAT(///15X28H STACK TEMP. EXCEEDS 450 F  )
      GO TO 2000
   12 IF(Q.GT.0.) GO TO 13
      RT=RT-DT
      S=RT
      DT1=DT/10.0
      RT1=RT+DT1
   21 X2=-TANH((G*(RT1-T0))/64.0)
      T=-B/(2.0*C)+(G/(2.0*C))*((X1+X2)/(1.0+X1*X2))
      RT=RT1
      XXXX=TBPLO-.001
      IF(T.GT.XXXX) GO TO 22
      RT=RT-DT1
      DT1=DT1/10.0
      RT1=RT+DT1
      GO TO 21
   22 YYYY=TBPLO+.001
      IF(T.LT.YYYY) GO TO 15
      RT1=RT1+DT1
      GO TO 21
   15 PCH2O=61.78-0.0997*T+PW
      IF (I2.LT.5.0) GO TO 41
      E=(CAHI*T+CBHI)*I2+(CDHI*T+CEHI)-0.2473*(PCH2O-27.0)
      GO TO 42
   41 E=(CALO*T+CBLO)*I2+(CDLO*T+CELO)-0.2473*(PCH2O-27.0)
   42 T1=T
      BP=0.0
      IHTR=0.0
```

```
      WRITE(6,1000)RT1,I2,E,T,BP,PCH2O,IHTR
      IF(RT1.GE.TIME2) GO TO 60
      RT=S+DT
      T1=TBPLO
      T0=RT1
      IF(T.LE.THON)GO TO 16
      IHTR=0.0
      IF(I2.GE.5.0) GO TO 25
      TR=(0.681*I2+2261.)/(8.841E-03*I2+13.3)
      GAMA=(2.70+22.976E-03*I2)/3.51
      Pw=60./(1.+8.94/GAMA)
      AGAMA=-8.601-14.838/(1.0+8.94/GAMA)
      TSS=(-3.413*CBLO*I2**2+(133.3-3.413*CELO-3.413*AGAMA)*I2+13.0*
     1-EPR)*TR-QB)/(3.413*CALO*I2**2+(.09459+3.413*CDLO)*I2+13.0*(1
     2R)+QA)
      PCH2O=61.78-0.0997*TSS+PW
      ESS=(CALO*TSS+CBLO)*I2+(CDLO*TSS+CELO)-0.2473*(PCH2O-27.0)
      A=32.0
      B=13.3*(1.0-EPR)+(3.413*CALO)*I2**2+(3.413*CDLO+3.413*0.0247)*
     1A
      LAMBDA=B/A
   27 T=TSS-(TSS-T1)*EXP(-LAMBDA*(RT-T0))
      PCH2O=61.78-0.0997*T+PW
      E=(CALO*T+CBLO)*I2+(CDLO*T+CELO)-0.2473*(PCH2O-27.0)
      BP=0.0
      IF(T.GT.TBPLO) GO TO 32
      IF(T.LE.THON) GO TO 33
      IF(T.LT.350.) GO TO 24
      WRITE(6,1000)RT,I2,E,T,BP,PCH2O,IHTR
      IF(RT.GE.TIME2) GO TO 60
      RT=RT+DT
      GO TO 27
   25 TR=(0.681*I2+2261.)/(8.841E-03*I2+13.3)
      GAMA=(2.70+22.976E-03*I2)/3.51
      PW=60.0/(1.0+8.94/GAMA)
      AGAMA=-8.601-14.838/(1.0+8.94/GAMA)
      TSS=(-3.413*CBHI*I2**2+(133.3-3.413*CEHI-3.413*AGAMA)*I2+13.0*
     1-EPR)*TR-QB)/(3.413*CAHI*I2**2+(.09459+3.413*CDHI)*I2+13.0*(1
     2R)+QA)
      PCH2O=61.78-0.0997*TSS+PW
      ESS=(CAHI*TSS+CBHI)*I2+(CDHI*TSS+CEHI)-0.2473*(PCH2O-27.0)
      A=32.0
      B=13.3*(1.0-EPR)+(3.413*CAHI)*I2**2+(3.413*CDHI+0.09459)*I2+0.
      LAMBDA=B/A
   18 T=TSS-(TSS-T1)*EXP(-LAMBDA*(RT-T0))
      PCH2O=61.78-0.0997*T+PW
      E=(CAHI*T+CBHI)*I2+(CDHI*T+CEHI)-0.2473*(PCH2O-27.0)
      BP=0.0
      IF(T.GT.TBPLO) GO TO 37
      IF(T.LE.THON) GO TO 36
      WRITE(6,1000)RT,I2,E,T,BP,PCH2O,IHTR
      IF(RT.GE.TIME2) GO TO 60
      RT=RT+DT
      GO TO 18
   37 TB=TBPLO
      IHTR=0.0
```

```
      GO TO 19
   36 TB=THON
      IHTR=5.15
      GO TO 19
   33 TIME=T0-(1./LAMBDA)*ALOG((TSS-THON)/(TSS-T1))
      T=THON
      PCH20=61.78-0.0997*T+PW
      IHTR=5.15
      I=I2+IHTR
      E=(CALO*T+CBLO)*I2+(CDLO*T+CELO)-0.2473*(PCH20-27.0)
      BP=0.0
      WRITE(6,1000)TIME,I2,E,T,BP,PCH20,IHTR
      E=(CALO*T+CBLO)*I +(CDLO*T+CELO)-0.2473*(PCH20-27.0)
      WRITE(6,1000)TIME,I ,E,T,BP,PCH20,IHTR
      T1=T
      T0=TIME
      HTIME=TIME
      GO TO 26
   32 TIME=T0-(1./LAMBDA)*ALOG((TSS-TBPLO)/(TSS-T1))
      T=TBPLO
      PCH20=61.78-0.0997*T+PW
      E=(CALO*T+CBLO)*I2+(CDLO*T+CELO)-0.2473*(PCH20-27.0)
      BP=0.0
      WRITE(6,1000)TIME,I2,E,T,BP,PCH20,IHTR
      T1=T
      T0=TIME
      IF(TIME.GE.TIME2) GO TO 60
      GO TO 17
   16 IHTR=5.15
      I=I2+5.15
      TR=(0.681*I+2261.)/(8.841E-03*I+13.3)
      GAMA=(2.70+22.976E-03*I)/3.51
      PW=60./(1.+8.94/GAMA)
      AGAMA=-8.601-14.838/(1.0+8.94/GAMA)
      TSS=(13.3*(1.0-EPR)*TR+544.8-QB+133.3*I-3.413*I*(CBHI*I+CEHI+,
     1))/(13.3*(1.0-EPR)+0.01043*I+3.413*I*(CAHI*I+CDHI+.02466)+QA)
      PCH20=61.78-0.0997*TSS+PW
      ESS=(CAHI*TSS+CBHI)*I+(CDHI*TSS+CEHI)-0.2473*(PCH20-27.0)
      A=32.0
      B=13.3*(1.0-EPR)+3.413*CAHI*I**2+(3.413*CDHI+0.09459)*I+QA
      LAMBDA=B/A
      DELHT=RT-TIME
   23 T=TSS-(TSS-T1)*EXP(-LAMBDA*(RT-T0))
      PCH20=61.78-0.0997*T+PW
      E=(CAHI*T+CBHI)*I+(CDHI*T+CEHI)-0.2473*(PCH20-27.0)
      BP=0.0
      IF(T.GT.THOF) GO TO 30
      IF(T.LT.350.0) GO TO 24
      WRITE(6,1000)RT,I2,E,T,BP,PCH20,IHTR
      IF(RT.GE.TIME2) GO TO 31
      RT=RT+DT
      DELHT=DELHT+DT
      GO TO 23
   31 WRITE(6,1004) DELHT
      GO TO 60
   30 TIME=T0-(1.0/LAMBDA)*ALOG((TSS-THOF)/(TSS-T1))
```

```
      DELHT=DELHT-(RT-TIME)
      T=THOF
      PCH2O=61.78-0.0997*T+PW
      IHTR=5.15
      I=I2+IHTR
      E=(CAHI*T+CBHI)*I +(CDHI*T+CEHI)-0.2473*(PCH2O-27.0)
      BP=0.0
      WRITE(6,1000)TIME,I ,E,T,BP,PCH2O,IHTR
      E=(CAHI*T+CBHI)*I2+(CDHI*T+CEHI)-0.2473*(PCH2O-27.0)
      WRITE(6,1000)TIME,I2,E,T,BP,PCH2O,IHTR
      WRITE(6,1004) DELHT
      T0=TIME
   26 T1=T
      IF(TIME.GE.TIME2) GO TO 60
      GO TO 3
   19 TIME=T0-(1./LAMBDA)*ALOG((TSS-TB)/(TSS-T1))
      T=TB
      PCH2O=61.78-0.0997*T+PW
      E=(CAHI*T+CBHI)*I2+(CDHI*T+CEHI)-0.2473*(PCH2O-27.0)
      BP=0.0
      WRITE(6,1000)TIME,I2,E,T,BP,PCH2O,IHTR
      T1=T
      T0=TIME
      IF(TIME.GE.TIME2) GO TO 60
      IF(T.LE.400.) GO TO 16
      GO TO 17
   20 WRITE(6,2003)
 2003 FORMAT(///15X31H DISCRIMINANT IS LESS THAN ZERO)
      GO TO 2000
    7 WRITE(6,2004)
 2004 FORMAT(///15X25H DISCRIMINANT EQUALS ZERO)
      GO TO 2000
   13 X3=ATAN(((2.0*C*420.0)+B)/G)
      X4=ATAN(((2.0*C*T1)+B)/G)
      TIME=T0+(64.0/G)*(X3-X4)
      T=TBPLO
      RT1=TIME
      GO TO 15
    8 THETA1=ATAN((2.0*C*T1+B)/SQRT(Q))
      THETA2=(SQRT(Q)*(RT-T0))/64.0
      THETA=THETA1+THETA2
      TAN=SIN(THETA)/COS(THETA)
      T=(-B)/(2.0*C)+(SQRT(Q)/(2.0*C))*TAN
      PCH2O=61.78-0.0997*T+PW
      IF(I2.LT.5.0) GO TO 43
      E=(CAHI*T+CBHI)*I2+(CDHI*T+CEHI)-0.2473*(PCH2O-27.0)
      GO TO 44
   43 E=(CALO*T+CBLO)*I2+(CDLO*T+CELO)-0.2473*(PCH2O-27.0)
   44 G=SQRT(Q)
      GO TO 11
   24 WRITE(6,2005)
 2005 FORMAT(///15X27H STACK TEMP. IS BELOW 350 F)
      GO TO 2000
   60 PSS=ESS*I2
      TIME1=TIME2
      I1=I2
```

```
      T1=T
      WRITE(6,1001)TSS
      WRITE(6,1002)ESS
      WRITE(6,1003)PSS
      GO TO 5
  999 FORMAT(7X4HTIME7X1HI11X1HE11X1HT8X2HBP5X4HCONC5X4HIHTR/7X3HHR
     1AMPS7X5HVOLTS7X4HDEGF6X5HPRCNT2X7HPRCTH203X4HAMPS)
 5000 FORMAT(//4F15.7)
 1000 FORMAT(F12.4,2F11.4,F12.4,F8.2,F9.2,F8.2)
 1001 FORMAT(//14X20H TEMP STEADY STATE = F13.8)
 1002 FORMAT(14X24H VOLTAGE STEADY STATE = F13.8)
 1003 FORMAT(14X22H POWER STEADY STATE = F13.8//////)
 1004 FORMAT(//14X10HHTR ON FORF9.4,4H HRS)
 3000 FORMAT(14F8.3)
 2000 CONTINUE
      END
```

REFERENCES

1. Wood, Jessie H.; and Keenan, Charles W.: General College Chemistry. Harper and Brothers, Pubs., 1957, p. 462.

2. Young, George J., ed.: Fuel Cells. Vol. I. Am. Chem. Soc., Reinhold Pub. Corp., 1960, p. 6.

3. Chang, Sheldon S. L.: Energy Conversion. Ch. 7. Prentice-Hall, Inc., 1963.

4. Arthur, R. A.: Chemistry for Today — A Basic Course. Cambridge Book Co., 1958, p. 231.

5. Mooney, David A.: Mechanical Engineering Thermodynamics. Prentice-Hall, Inc., 1953, pp. 170 and 504.

6. Weber, Harold C.; and Meissner, Herman P.: Thermodynamics for Chemical Engineers. John Wiley and Sons, Inc., 1959, p. 102.

7. Glasstone, Samuel: Thermodynamics for Chemists. D. van Nostrand Co., Inc., 1947, p. 79.

8. Keenan, Joseph H.; and Kaye, Joseph: Gas Tables. John Wiley and Sons, Inc., 1948.

9. Van Wylen, Gordon J.: Thermodynamics. Ch. 9. John Wiley and Sons, Inc., 1959.

10. Jakob, Max; and Hawkins, George A.: Elements of Heat Transfer. Third ed., John Wiley and Sons, Inc., 1957, p. 185.

NASA-Langley, 1968 — 3 S-163

NATIONAL AERONAUTICS AND SPACE ADMINISTRATION
WASHINGTON, D. C. 20546
OFFICIAL BUSINESS

FIRST CLASS MAIL

POSTAGE AND FEES PAID
NATIONAL AERONAUTICS AND
SPACE ADMINISTRATION

POSTMASTER: If Undeliverable (Section 158 Postal Manual) Do Not Return

"The aeronautical and space activities of the United States shall be conducted so as to contribute . . . to the expansion of human knowledge of phenomena in the atmosphere and space. The Administration shall provide for the widest practicable and appropriate dissemination of information concerning its activities and the results thereof."

—NATIONAL AERONAUTICS AND SPACE ACT OF 1958

NASA SCIENTIFIC AND TECHNICAL PUBLICATIONS

TECHNICAL REPORTS: Scientific and technical information considered important, complete, and a lasting contribution to existing knowledge.

TECHNICAL NOTES: Information less broad in scope but nevertheless of importance as a contribution to existing knowledge.

TECHNICAL MEMORANDUMS: Information receiving limited distribution because of preliminary data, security classification, or other reasons.

CONTRACTOR REPORTS: Scientific and technical information generated under a NASA contract or grant and considered an important contribution to existing knowledge.

TECHNICAL TRANSLATIONS: Information published in a foreign language considered to merit NASA distribution in English.

SPECIAL PUBLICATIONS: Information derived from or of value to NASA activities. Publications include conference proceedings, monographs, data compilations, handbooks, sourcebooks, and special bibliographies.

TECHNOLOGY UTILIZATION PUBLICATIONS: Information on technology used by NASA that may be of particular interest in commercial and other non-aerospace applications. Publications include Tech Briefs, Technology Utilization Reports and Notes, and Technology Surveys.

Details on the availability of these publications may be obtained from:

SCIENTIFIC AND TECHNICAL INFORMATION DIVISION

NATIONAL AERONAUTICS AND SPACE ADMINISTRATION

Washington, D.C. 20546